INSTITUTE OF PHYSICS PUBLISHING REPORTS ON PROGRESS IN PHYSICS

Rep. Prog. Phys. **65** (2002) 251–297 PII: S0034-4885(02)93943-6

Fluorescence correlation spectroscopy: the technique and its applications

Oleg Krichevsky[1] **and Grégoire Bonnet**[2]

[1] Physics Department, Ben-Gurion University, Beer-Sheva 84105, Israel
[2] Laboratory of Immunology, Building 10/11N308 NIAID/NIH, Bethesda, MD 20892, USA

E-mail: okrichev@bgumail.bgu.ac.il

Received 25 June 2001, in final form 3 December 2001
Published 8 January 2002
Online at stacks.iop.org/RoPP/65/251

Abstract

Fluorescence correlation spectroscopy (FCS) is an experimental technique using statistical analysis of the fluctuations of fluorescence in a system in order to decipher dynamic molecular events, such as diffusion or conformational fluctuations of biomolecules. First introduced by Magde *et al* to measure the diffusion and binding of ethidium bromide onto double-stranded DNA, the technique has been undergoing a renaissance since 1993 with the implementation of confocal microscopy FCS. Since then, a flurry of experiments has implemented FCS to characterize the photochemistry of dyes, the translational and rotational mobilities of fluorescent molecules, as well as to monitor conformational fluctuations of green fluorescent proteins and DNA molecules.

In this review, we present the analytical formalism of an FCS measurement, as well as practical considerations for the design of an FCS setup and experiment. We then review the recent applications of FCS in analytical chemistry, biophysics and cell biology, specifically emphasizing the advantages and pitfalls of the technique compared to alternative spectroscopic tools. We also discuss recent extensions of FCS in single-molecule spectroscopy, offering alternative data processing of fluorescence signals to glean more information on the kinetic processes.

(Some figures in this article are in colour only in the electronic version)

Contents

1. Introduction

Fluorescence correlation spectroscopy (FCS) is an experimental technique, developed to study kinetic processes through the statistical analysis of equilibrium fluctuations. A fluorescence signal is coupled to the different states of the system of interest, so that spontaneous fluctuations in the system's state generate variations in fluorescence. The autocorrelation function of fluctuations in fluorescence emission carries information on the characteristic time scales and the relative weights of different transitions in the system. Thus, with the appropriate model of the system dynamics, different characteristic kinetic rates can be measured. For example, fluctuations in the number of fluorescent particles unravel the diffusion dynamics in the sampling volume.

Since its invention in 1972 by Magde *et al* (1972), FCS has known the classical age: chemical rates of binding–unbinding reactions as well as coefficients of translational and rotational diffusion have been measured (for a review of this period see Thompson (1991)). However, although the principal ideas behind FCS as well as its main applications were already established at that stage, the technique was still rather cumbersome and poorly sensitive, requiring high concentrations of fluorescent molecules. Its renaissance came in 1993 with the introduction of the confocal illumination scheme in FCS by Rigler *et al* (1993). This work generated a flurry of technical improvements, pushed the sensitivity of the technique to the single-molecule level and led to a renewed interest in FCS. The efficient detection of emitted photons extended the range of applications and allowed one to probe the conformational fluctuations of biomolecules and the photodynamical properties of fluorescent dyes. Finally, FCS recently entered the industrial age with the introduction of Zeiss and Evotech's Confocor commercial instrument, and its common use in drug-screening assays.

A number of recent short reviews (Eigen and Rigler 1994, Berland 1997, Maiti *et al* 1997, Auer *et al* 1998) on the different aspects of FCS attest to the popularity of the technique. A book on FCS by Rigler and Elson (2001) has been announced as well, but at the time of writing this review has not yet been released.

In this review we attempt to summarize the progress in FCS experiments during the past decade. Although until now FCS has been used almost exclusively in the domains of biophysics and biology, we will try to present those applications which could be of interest to physicists, at least to those who are motivated by biological problems. Having in mind that between the development of the theoretical framework of FCS and the bulk of FCS measurements there was a time interval of two decades, we decided to also review the formalism of FCS by Elson and Magde (1974), adapted to the modern experimental situation. However, we would like to start with a brief historical overview of the precursors to FCS as well as the classical FCS experiments by Magde *et al* (1972).

1.1. Historical lineage

FCS is a technique which relies on the fact that thermal noise, usually a source of annoyance in an experimental measurement, can be used to the profit of an experimentalist to glean some information on the system under study.

The understanding of the fluctuation–relaxation relationship in thermodynamics has been a great achievement of statistical physics. The theory of Brownian movement, presented by Einstein in one of his famous 1905 papers (Einstein 1905), not only established a macroscopic understanding of the consequences of the existence of the atom, but also opened up a whole new area of research related to the study of systems near equilibrium. The experimental support for this atomistic theory came with Perrin's observation of Brownian particles of mastic under a

microscope (Perrin 1914). Macroscopic dynamical properties (the viscosity of the fluid) were derived from microscopic fluctuations (the diffusion of the probe). It is humbling to point out that, right at the beginning of the 20th century, experimentalists had already figured out the importance of reducing the sample size and using high-power microscopy to unravel atomic wonders.

The explicit formulation of the fluctuation–dissipation theorem states that the dynamics governing the relaxation of a system out of equilibrium are embedded in the equilibrium statistics. In the spirit of this theory, Eigen and followers developed the temperature-jump technique, where the relaxation of a system after thermal perturbation gives insight into the thermodynamic equilibrium. Classically, the temperature jump is generated by capacitance discharge or laser-pulse absorption, and the relaxation towards equilibrium is monitored by spectroscopy (e.g. UV absorption or circular dichroism).

Another perturbative technique has been introduced to measure the diffusion of biomolecules. Fluorescence recovery after photobleaching (FRAP), as its name implies, consists in monitoring the dynamics of fluorescence restoration after photolysis, due to the diffusion influx from neighbouring areas. This photodestructive method has been very successful in application to living cells, specifically to analyse the dynamics of membrane trafficking.

Less invasive techniques, such as quasi-elastic light scattering (QELS), are also used to get dynamic information from monitoring the fluctuations of the refraction index (Berne and Peccora 1976). However, QELS is poorly sensitive to changes on the molecular level, while the other techniques discussed (T jump and FRAP) are perturbative.

A widely used method to study changes on a molecular scale (10–100 Å) is based on the fluorescence resonance energy transfer (FRET): a transfer of an excitation between two different fluorophores (donor and acceptor), whose corresponding emission (donor) and excitation (acceptor) spectra overlap. The efficiency of energy transfer depends strongly on the distance between the donor and the acceptor: hence one can take advantage of FRET to follow the association of two interacting molecules or to monitor the distance between two sites within a macromolecule when labelled with two appropriate dyes (for a recent review see Hillisch *et al* (2001)).

FCS corrects the shortcomings of its precursors, as it monitors the relaxation of fluctuations around the equilibrium state in a non-invasive fashion. It relies on the robust and specific signal provided by fluorescent particles to analyse their motions and interactions. In combination with FRET, FCS further allows one to probe the dynamics of intra-molecular motions.

1.2. The first implementation of FCS by Magde et al (1972)

Magde *et al* (1972) invented FCS in 1972 and showed its feasibility by monitoring the fluctuations in the chemical equilibrium of the binding reaction of ethidium bromide to double-stranded DNA. Ethidium bromide (EtBr) is a small intercalating dye, whose fluorescence quantum yield increases by a factor of 20 upon insertion between DNA bases. Thus Magde *et al* (1972) studied the binding equilibrium

$$\mathrm{EtBr} + \mathrm{DNA} \underset{k_{\mathrm{debinding}}}{\overset{k_{\mathrm{binding}}}{\rightleftharpoons}} \mathrm{EtBr} \bullet \mathrm{DNA}$$

by monitoring the fluorescence fluctuations of the dye.

The original implementation of FCS used laser excitation of 6 kW cm^{-2} at 514.5 nm. Fluorescence was collected by a parabolic reflector, filtered from the scattered excitation light with a $K_2Cr_2O_7$ solution, and detected with a photomultiplier tube. The analogue fluorescence

signal was then analysed with two 100-channel correlators. The typical concentrations were 5 μmol for the ethidium bromide, and 5 nmol for the sonicated calf-thymus DNA of 20 kDa. The dimensions of the collection volume were 5 μm transversally and 150 μm longitudinally: thus there were about 10^4 molecules in the field of view. The resulting time scales of relaxation for the autocorrelation function of the collected fluorescence were in the 10–100 ms range.

There were two sources of fluorescence fluctuations in this experiment: diffusion of the molecules in/out of the sampling volume, and chemical fluctuations associated with the binding/debinding of EtBr. Correspondingly, the FCS autocorrelation function is a convolution of diffusion and chemical relaxation terms.

The relaxation rate R, characteristic of the binding/debinding, is deduced from the fits to the fluorescence autocorrelation function and is linearly dependent on the EtBr concentration ($R = k_{\text{binding}}$ ([EtBr] + [DNA]) + $k_{\text{debinding}} \approx k_{\text{binding}}$[EtBr] + $k_{\text{debinding}}$). This dependence was measured by Magde *et al* (1972) to yield

$$k_{\text{binding}} = 1.5 \times 10^7 \text{ M}^{-1} \text{ s}^{-1}$$
$$k_{\text{debinding}} = 27 \text{ s}^{-1}.$$

This benchmark experiment proved the feasibility of assessing parameters of chemical kinetics through the analysis of equilibrium fluctuations. It set the groundwork for the following implementations of FCS and other related techniques that are presented in this review.

In the following sections, the general formalism of FCS measurement will be introduced. Particular cases of experimental relevance will be considered, and the statistical accuracy of an FCS measurement discussed (section 2). We will then describe the modern experimental setups for FCS with practical considerations on their implementation (section 3). Modern applications of FCS to different experimental systems will be reviewed in section 4. Emphasis is put on the analysis of fluorescence photochemistry, the determination of translational and rotational mobilities, application in binding assays, the analysis of conformational fluctuations of biomolecules, and the measurement of biomolecular mobilities in living cells. Finally, in section 5, we will present the recently introduced techniques arising from FCS: the photon counting histogram and single-molecule imaging.

2. The theory of FCS

In this section we compute the autocorrelation function of the intensity of emission accounting for the physical and chemical fluctuations in the sample under study. Samples are maintained at thermal equilibrium so that all of the processes under analysis are in fact statistical fluctuations around equilibrium. The kinetic coefficients corresponding to these processes (e.g. diffusion coefficients and/or chemical rates) determine the dynamics of their relaxation, which in turn determines the shape of the intensity autocorrelation function $G(t)$.

We derive here the expression of $G(t)$ related to the kinetics of fluctuations. In the first subsection we present the general case of a system with many chemical components undergoing diffusion and chemical reactions. In principle, the kinetic coefficients for all of the processes contribute to the decay of $G(t)$, and so all of them can be determined from the autocorrelation function. In practice, however, mixing more than two or three processes in the system can make the experimental situation extremely confusing (unless the characteristic time scales of these processes are well separated). Hence, in the following subsections we will present a few simplified cases relevant to different experimental situations. Our presentation of the theory of FCS follows closely the line and the notation of the classical derivation by Elson and Magde (1974) with some minor modifications introduced.

2.1. General formalism

We consider here an ideal solution of m chemical components. We characterize component j by its local concentration $C_j(\vec{r},t)$, its ensemble average concentration $\bar{C}_j = \langle C_j(\vec{r},t)\rangle$ and the local deviation $\delta C_j(\vec{r},t) = C_j(\vec{r},t) - \bar{C}_j$. The components participate in diffusion and in chemical reactions converting some of the components into others. Near equilibrium, the nonlinear chemical equations can be linearized and the equation for the relaxation of δC_j can be written as

$$\frac{\partial \delta C_j(\vec{r},t)}{\partial t} = D_j \nabla^2 \delta C_j(\vec{r},t) + \sum_{k=1}^{m} K_{jk}\delta C_k(\vec{r},t) \tag{1}$$

where the first term accounts for diffusion and the second term describes the chemical changes, and where the coefficients K_{jk} are combined from the chemical rate constants and the equilibrium concentrations of the species.

The distribution of the excitation light in the sample is denoted by $I(\vec{r})$ (in fact, $I(\vec{r})$ is determined by both the illumination and the detection optical paths). We assume that the number of photons emitted and collected from each of the molecules is proportional to $I(\vec{r})$, so that the number of collected photons per sample time Δt is

$$n(t) = \Delta t \int \mathrm{d}^3\vec{r}\, I(\vec{r}) \sum_{k=1}^{m} Q_k C_k(\vec{r},t) \tag{2}$$

where Q_k is the product of the absorption cross section by the fluorescence quantum yield and the efficiency of fluorescence for the component k. Here, we do not consider shot noise as it is uncorrelated and does not contribute to $G(t)$ (but it does contribute to the noise on $G(t)$, see the discussion in section 2.5). Then the deviation $\delta n(t)$ of the photon count from the mean $\bar{n} = \langle n(t)\rangle$ is

$$\delta n(t) = n(t) - \bar{n} = \Delta t \int \mathrm{d}^3\vec{r}\, I(\vec{r}) \sum_{k=1}^{m} Q_k \delta C_k(\vec{r},t). \tag{3}$$

In FCS experiments, $G(t)$ is determined as a time average of the products of the intensity fluctuations and normalized by the square of the average intensity $\bar{n}^2$:

$$G(t) = \frac{1}{\bar{n}^2 T} \sum_{i=0}^{T-1} \delta n(t')\delta n(t'+t) \tag{4}$$

where T is the total number of accumulated sampling intervals Δt ($T\Delta t$ is the total duration of the experiment), t corresponds to delay channel m of the correlator such that $m = t/\Delta t$; $\delta n(t') = n_i - \bar{n}$, $\delta n(t'+t) = n_{i+m} - \bar{n}$, where n_i, n_{i+m} are the numbers of photon counts sampled at times $t' = i\Delta t$ and $t'+t = (i+m)\Delta t$, respectively.

For the purpose of derivation we will use the ergodicity of the system to write (4) as an ensemble average:

$$G(t) = \frac{1}{\bar{n}^2}\langle \delta n(0)\, \delta n(t)\rangle \tag{5}$$

Substituting (3) into (5) we obtain

$$G(t) = \frac{(\Delta t)^2}{\bar{n}^2} \iint \mathrm{d}^3\vec{r}\, \mathrm{d}^3\vec{r}'\, I(\vec{r}) I(\vec{r}') \sum_{j,l} Q_j Q_l \langle \delta C_j(\vec{r},0)\delta C_l(\vec{r}',t)\rangle. \tag{6}$$

Thus the autocorrelation function of intensity fluctuations is a convolution of the auto- and cross-correlation functions of the concentration fluctuations with the excitation profile.

In the following we will use the fact that $\delta C_l(\vec{r},t)$ are the solutions of equations (1) with the initial condition $\delta C_l(\vec{r},0)$ in order to express $\langle \delta C_j(\vec{r},0)\,\delta C_l(\vec{r}',t)\rangle$ through the combinations of zero-time correlations $\langle \delta C_j(\vec{r},0)\,\delta C_k(\vec{r}'',0)\rangle$. The latter can be evaluated from the condition of ideality of the chemical solution: the correlation length being much smaller than the distances between molecules, the positions of different molecules of the same species as well as those of different species are decorrelated:

$$\langle \delta C_j(\vec{r},0)\delta C_k(\vec{r}'',0)\rangle = \bar{C}_j\delta_{jk}\delta(\vec{r}-\vec{r}''). \tag{7}$$

$\bar{C}_j$ stands here for the mean-square fluctuations of the number $C_j(\vec{r},t)$ of molecules in a unit volume being equal to its average $\langle C_j(\vec{r},t)\rangle$ for Poisson statistics.

In order to obtain the solutions $\delta C_j(\vec{r},t)$ as a function of the initial conditions $\delta C_j(\vec{r},0)$ we apply a Fourier transform to equation (1):

$$\frac{\mathrm{d}\tilde{C}_l(\vec{q},t)}{\mathrm{d}t} = \sum_{k=1}^{m} M_{lk}\tilde{C}_k(\vec{q},t) \tag{8}$$

where $\tilde{C}_l(\vec{q},t) = (2\pi)^{-3/2}\int \mathrm{d}^3\vec{r}\,\mathrm{e}^{\mathrm{i}\vec{q}\vec{r}}\delta C_l(\vec{r},t)$ is a Fourier transform of $\delta C_l(\vec{r},t)$, and $M_{lk} = T_{lk} - D_l q^2\delta_{lk}$. The solutions of (8) can be represented in a standard way through the eigenvalues $\lambda^{(s)}$ and the corresponding eigenvectors $X^{(s)}$ of the matrix $\boldsymbol{M}$:

$$\tilde{C}_l(\vec{q},t) = \sum_{s=1}^{m} X_l^{(s)} h_s \exp(\lambda^{(s)}t). \tag{9}$$

The coefficients h_s are to be found from the initial conditions: $\tilde{C}_l(\vec{q},0) = \sum_{s=1}^{m} X_l^{(s)}h_s$. Hence, $h_s = \sum_{k=1}^{m}(X^{-1})_k^{(s)}\tilde{C}_k(\vec{q},0)$ and

$$\tilde{C}_l(\vec{q},t) = \sum_{s=1}^{m} X_l^{(s)}\exp(\lambda^{(s)}t)\sum_{k=1}^{m}(X^{-1})_k^{(s)}\tilde{C}_k(\vec{q},0) \tag{10}$$

where X^{-1} is the inverse matrix of eigenvectors. Taking into account the fact that the Fourier transform and the ensemble averaging are independent linear operations and thus can be applied in any order, and making use of (10) and (7), we can evaluate

$$\begin{aligned}
\langle \delta C_j(\vec{r},0)\delta C_l\left(\vec{r}',t\right)\rangle &= (2\pi)^{-3/2}\int \mathrm{d}^3\vec{q}\,\mathrm{e}^{-\mathrm{i}\vec{q}\vec{r}'}\langle \delta C_j(\vec{r},0)\,\delta C_l(\vec{q},t)\rangle \\
&= (2\pi)^{-3/2}\int \mathrm{d}^3\vec{q}\,\mathrm{e}^{-\mathrm{i}\vec{q}\vec{r}'}\sum_{s=1}^{m} X_l^{(s)}\exp(\lambda^{(s)}t)\sum_{k=1}^{m}(X^{-1})_k^{(s)}\langle \delta C_j(\vec{r},0)\,\tilde{C}_k(\vec{q},0)\rangle \\
&= (2\pi)^{-3}\int \mathrm{d}^3\vec{q}\,\mathrm{e}^{-\mathrm{i}\vec{q}\vec{r}'}\sum_{s=1}^{m} X_l^{(s)}\exp(\lambda^{(s)}t)\sum_{k=1}^{m}(X^{-1})_k^{(s)} \\
&\quad\times\int \mathrm{d}^3\vec{r}''\,\mathrm{e}^{\mathrm{i}\vec{q}\vec{r}''}\langle \delta C_j(\vec{r},0)\delta\tilde{C}_k(\vec{r}'',0)\rangle \\
&= (2\pi)^{-3}\,\bar{C}_j\int \mathrm{d}^3\vec{q}\,\mathrm{e}^{\mathrm{i}\vec{q}(\vec{r}-\vec{r}')}\sum_{s=1}^{m} X_l^{(s)}\exp(\lambda^{(s)}t)(X^{-1})_j^{(s)}.
\end{aligned} \tag{11}$$

Finally, substituting (11) into (6) and carrying out the integration over $\vec{r}$ and $\vec{r}'$, we obtain

$$G(t) = \frac{(\Delta t)^2}{\bar{n}^2}\int \mathrm{d}^3\vec{q}\,|\tilde{I}(\vec{q})|^2\sum_{j,l} Q_j Q_l\bar{C}_j\sum_{s} X_l^{(s)}\exp(\lambda^{(s)}t)(X^{-1})_j^{(s)} \tag{12}$$

where $\tilde{I}(\vec{q}) = (2\pi)^{-3/2}\int \mathrm{d}^3\vec{r}\,\mathrm{e}^{-\mathrm{i}\vec{q}\vec{r}}I(\vec{r})$ is the Fourier transform of $I(\vec{r})$. The average number $\bar{n}$ of the collected photons in (12) is determined from (2):

$$\bar{n} = \Delta t\int \mathrm{d}^3r\,I(\vec{r})\sum_{i=1}^{m} q_i\bar{C}_i = (2\pi)^{3/2}\,\tilde{I}(0)\,\Delta t\sum_{i=1}^{m} q_i\bar{C}_i. \tag{13}$$

Thus $G(t)$ can be evaluated from the parameters of the experimental setup and from diffusion coefficients, chemical rates and concentrations of the chemical components of a sample.

In many realizations of FCS, a confocal illumination/detection optical setup is used such that $G(t)$ can be calculated explicitly by assuming a Gaussian illumination intensity profile:

$$I(\vec{r}) = I_0 \exp\left(-\frac{2\left(x^2+y^2\right)}{w_{xy}^2} - \frac{2z^2}{w_z^2}\right) \tag{14}$$

where w_z and w_{xy} are the sizes of the beam waist in the direction of the propagation of light and in the perpendicular direction, respectively (normally $w_z > w_{xy}$).

Then, the Fourier transform of the illumination/collection profile is

$$\tilde{I}(\vec{q}) = \frac{I_0 w_{xy}^2 w_z}{8} \exp\left(-\frac{w_{xy}^2}{8}\left(q_x^2+q_y^2\right) - \frac{w_z^2}{8}q_z^2\right) \tag{15}$$

and from (12), (13) and (15):

$$G(t) = \frac{(2\pi)^{-3}}{\left(\sum Q_i \bar{C}_i\right)^2} \int \mathrm{d}^3\vec{q}\, \exp\left(-\frac{w_{xy}^2}{4}\left(q_x^2+q_y^2\right) - \frac{w_z^2}{4}q_z^2\right) \times \sum_{j,l} Q_j Q_l \bar{C}_j \sum_s X_l^{(s)} \exp(\lambda^{(s)}t)(X^{-1})_j^{(s)}. \tag{16}$$

For each particular case $G(t)$ can be computed from the general expression (16) by evaluating the $\vec{q}$ dependence of the eigenvalues for the relaxation dynamics.

2.2. *Single-component diffusion*

We start by applying the general formalism to the simplest possible case: diffusion of a single chemical species in a dilute solution. Then the system of equation (1) consists of a single diffusion equation (we omit in this case all of the subscripts):

$$\frac{\partial \delta C(\vec{r},t)}{\partial t} = D\nabla^2 \delta C(\vec{r},t)$$

which can be easily solved by taking a Fourier transform:

$$\delta C(\vec{q},t) = \delta C(\vec{q},0)\exp(-Dq^2 t).$$

The matrix M has just one eigenvalue, $\lambda = -Dq^2$, and its only eigenvector is trivially $X = 1$. Substituting these values into (16) yields

$$G(t) = \frac{(2\pi)^{-3}}{Q^2\bar{C}^2} \int \mathrm{d}^3\vec{q}\, Q^2\bar{C} \exp\left(-\frac{w_{xy}^2}{4}\left(q_x^2+q_y^2\right) - \frac{w_z^2}{4}q_z^2 - Dt\left(q_x^2+q_y^2+q_z^2\right)\right) = \frac{1}{\bar{C}V}\left(1+\frac{t}{\tau_D}\right)^{-1}\left(1+\frac{t}{\tau_D'}\right)^{-1/2} \tag{17}$$

where $V = \pi^{3/2} w_{xy}^2 w_z$ is an effective sampling volume, and $\tau_D = w_{xy}^2/4D$ and $\tau_D' = w_z^2/4D$ are, respectively, the characteristic times of diffusion across and along the illuminated region. Finally, denoting the average number of molecules in the sampling volume as $\bar{N} = V\bar{C}$ and the aspect ratio of the sampling volume as $\omega = w_z/w_{xy}$, we obtain

$$G(t) = \frac{1}{\bar{N}}\left(1+\frac{t}{\tau_D}\right)^{-1}\left(1+\frac{t}{\omega^2\tau_D}\right)^{-1/2}. \tag{18}$$

As we could expect, the amplitude of the correlation function is inversely proportional to the average number of molecules in the sampling volume, since the fluctuations $\delta N/\bar{N}$ in the

number of molecules in the sampling volume are inversely proportional to $\sqrt{\bar{N}}$ and since $G(t)$ is second order in the intensity of fluorescence.

Notice that in (17) and (18) each of the directions of translational motion brings in a term like $(1 + t/\tau)^{-1/2}$, so that for a two-dimensional diffusion in the xy plane we have

$$G(t) = \frac{1}{\bar{N}} \frac{1}{1 + t/\tau_D}. \tag{19}$$

In practice, (19) is also a good approximation to a 3D system with the illumination conditions such that $\omega^2 \gg 1$ ($\tau_D \ll \tau'_D$), so that the relaxation of the fluctuations of the number of molecules in the sampling volume is determined by the rate of diffusion in the smaller dimensions.

Thus, the concentration and the diffusion coefficient of a fluorescent species can be evaluated with the help of equations (18) and (19) from the FCS measurement of $G(t)$, provided the dimensions of the sampling volume are calibrated in a separate experiment.

2.3. Multi-component diffusion

In the case of a dilute solution of two non-interacting species the equations in (1) consist of two independent diffusion equations for each of the species. The matrix M has two eigenvalues $\lambda^{(1)} = -D_1 q^2$ and $\lambda^{(2)} = -D_2 q^2$ and the trivial eigenvectors $X^{(1)} = \binom{1}{0}$ and $X^{(2)} = \binom{0}{1}$. Then, in the sums under the integral in (16), the terms corresponding to different species separate and the integration leads to

$$G(t) = \frac{Q_1^2 \bar{N}_1}{\left(Q_1 \bar{N}_1 + Q_2 \bar{N}_2\right)^2} \left(1 + \frac{t}{\tau_{D1}}\right)^{-1} \left(1 + \frac{t}{\omega^2 \tau_{D1}}\right)^{-1/2} + \frac{Q_2^2 \bar{N}_2}{\left(Q_1 \bar{N}_1 + Q_2 \bar{N}_2\right)^2} \left(1 + \frac{t}{\tau_{D2}}\right)^{-1} \left(1 + \frac{t}{\omega^2 \tau_{D2}}\right)^{-1/2} \tag{20}$$

where $\bar{N}_i = V\bar{C}_i$ is the average number of molecules of type 1 and 2 in the sampling volume $V = \pi^{3/2} w_{xy}^2 w_z$ with aspect ratio $\omega = w_z/w_{xy}$, and $\tau_{D1} = w_{xy}^2/4D_1$, $\tau_{D2} = w_{xy}^2/4D_2$ are the diffusion time scales of the species across the sampling volume.

Equation (20) can be obtained in a more intuitive way by considering the contributions n_1 and n_2 of each of the species to the total fluorescence. Then

$$G(t) = \frac{\langle (\delta n_1(0) + \delta n_2(0))(\delta n_1(t) + \delta n_2(t)) \rangle}{(\bar{n}_1 + \bar{n}_2)^2} = \frac{\langle \delta n_1(0)\, \delta n_1(t) \rangle}{(\bar{n}_1 + \bar{n}_2)^2} + \frac{\langle \delta n_2(0)\, \delta n_2(t) \rangle}{(\bar{n}_1 + \bar{n}_2)^2}$$
$$= \frac{\bar{n}_1^2}{(\bar{n}_1 + \bar{n}_2)^2} G_1(t) + \frac{\bar{n}_2^2}{(\bar{n}_1 + \bar{n}_2)^2} G_2(t) \tag{21}$$

where we made use of the independence of the species and $G_1(t) = \frac{\langle \delta n_1(0) \delta n_1(t) \rangle}{\bar{n}_1^2}$ and $G_1(t) = \frac{\langle \delta n_1(0) \delta n_1(t) \rangle}{\bar{n}_1^2}$ are the separate correlation functions of each of the components which are described by equation (18). Substituting $\bar{n}_1 = Q_1 \bar{N}_1$, $\bar{n}_2 = Q_2 \bar{N}_2$ and (18) into (21) we recover equation (20).

Equation (20) can easily be generalized for the case of many diffusing non-interacting components. Then

$$G(t) = \frac{1}{\left(\sum Q_k \bar{N}_k\right)^2} \sum Q_j^2 \bar{N}_j \left(1 + \frac{t}{\tau_{Dj}}\right)^{-1} \left(1 + \frac{t}{\omega^2 \tau_{Dj}}\right)^{-1/2}.$$

Note that the amplitude of the contribution of each species i in the autocorrelation function is weighted by its quantum yield Q_i. Thus, a measurement of the concentration for each of the species implies prior knowledge of Q_i.

2.4. Chemical reaction coupled with diffusion: isomerization case

We refer to Magde *et al* (1974) for the treatment of a more general case of a chemical reaction and restrict ourselves here to the simplest case of the chemical reaction, that of unimolecular isomerization (Berne and Peccora 1976):

$$A \underset{k_{BA}}{\overset{k_{AB}}{\rightleftarrows}} B\,.$$

We will assume, in addition, that the state A is fluorescent while the state B is non-fluorescent ($Q_B = 0, Q_A = Q$) and that the diffusion coefficient of molecules does not change upon isomerization: $D_A = D_B = D$. While these conditions might seem to be too restrictive, they are quite often met in experiments, as is discussed in the following sections, and the case overall is very illustrative.

Equations (1) for the present case are the following:

$$\begin{aligned}\frac{\partial \delta C_A(\vec{r},t)}{\partial t} &= D\nabla^2 \delta C_A(\vec{r},t) - k_{AB}\delta C_A + k_{BA}\delta C_B \\ \frac{\partial \delta C_B(\vec{r},t)}{\partial t} &= D\nabla^2 \delta C_B(\vec{r},t) + k_{AB}\delta C_A - k_{BA}\delta C_B.\end{aligned} \tag{22}$$

The matrix $\boldsymbol{M}$, corresponding to (22), is

$$M = \begin{bmatrix} -(Dq^2 - k_{AB}) & k_{BA} \\ k_{AB} & -(Dq^2 - k_{BA}) \end{bmatrix}.$$

Its eigenvalues are $\lambda^{(1)} = -q^2 D$ and $\lambda^{(2)} = -q^2 D - k_{AB} - k_{BA}$, and the eigenvectors are $X^{(1)} = \binom{1}{k_{AB}/k_{BA}}$ and $X^{(2)} = \binom{1}{-1}$. Substituting these values into (16) and taking into account that only the A state is fluorescent we obtain

$$G(t) = \frac{1}{\bar{N}}\left(1 + \frac{t}{\tau_D}\right)^{-1}\left(1 + \frac{t}{\omega^2\tau_D}\right)^{-1/2}\left(1 + K\exp\left(-\frac{t}{\tau}\right)\right) \tag{23}$$

where $\bar{N} = \left(\bar{C}_A + \bar{C}_B\right)V$ is the average total number of molecules in the sampling volume, $K = k_{AB}/k_{BA} = \bar{C}_B/\bar{C}_A$ is the equilibrium constant of the chemical reaction, $\tau = (k_{AB} + k_{BA})^{-1}$ is the relaxation time of the chemical reaction and $\tau_D = w_{xy}^2/4D$ is the characteristic diffusion time scale as before.

Thus, in this particular case, where the chemical reaction does not influence the rate of diffusion, the two processes involved, diffusion and isomerization, are independent and $G(t)$ is represented by the product of the term related to diffusion (18) and the term describing chemical relaxation.

We notice that for very short time delays $t \ll \tau, \tau_D$ the amplitude of the correlation function is determined by the average number of *fluorescent* molecules $\bar{N}_A = \bar{C}_A V$ in the sampling volume: $G(t \to 0) = 1/\bar{N}_A$. If the chemical kinetics is faster than diffusion ($\tau \ll \tau_D$), then for time delays longer than τ the correlation function approaches the shape of a correlation function for diffusion only (18) with the amplitude determined by the *total* number of molecules $\bar{N}$: in this time range all of the molecules appear to be fluorescent due to the fast turnover between the A and B states.

Finally, notice that the kinetics of diffusion and the chemical kinetics are described in (23) by very different functions: exponential decay for the chemical kinetics and an algebraic function for diffusion.

The formalism of Elson and Magde (1974) presented in this section is general enough to be applicable to most FCS experiments. The convolution of the diffusion–reaction equations

of chemical fluctuations with the spatial profile of the fluorescence excitation–collection yields analytical formulae to be used as fits in FCS experiments (see section 4 for applications).

2.5. Statistical accuracy in FCS

In this section, we discuss the statistical accuracy of an FCS measurement. In the simple case of diffusing molecules, the statistical reliability of the FCS method is tested for different concentrations of fluorescent molecules.

The rate of photon emission (and hence that of detection $n(t)$) being proportional to the average number of fluorescent molecules $\bar{N}$ in the sampling volume, the accumulated photon statistics will be better and hence the statistical noise will be smaller for *large* $\bar{N}$ (i.e. for high concentrations of molecules). On the other hand, the amplitude of the correlation function is inversely proportional to $\bar{N}$ (see, e.g., (18) and (23)), so that the signal itself will be larger at *small* concentrations. Is there any optimal concentration yielding the most accurate FCS measurement?

The question of statistics in FCS measurements was first addressed by Koppel (1974). It appears that, in a wide range of concentrations, the two effects discussed cancel each other exactly: the signal-to-noise (S/N) ratio is, in fact, independent of the solute concentration, but depends strongly on the rate of photon detection per molecule. We refer the reader to Koppel (1974) for a rigorous derivation as well as to the more recent papers by Qian (1990) and Kask *et al* (1997), and restrict ourselves here to an intuitive treatment of the case most relevant to the experimental situation: that of significant numbers of molecules in the sampling volume ($\bar{N} \gg 1$) and of low photon detection rate per molecule.

The signal-to-noise ratio in the FCS measurement is defined (Koppel 1974) as $S/N = G(t)/(\mathrm{var}\,(G(t)))^{1/2}$. From (4)

$$G(t) = \frac{1}{T}\sum_{i=0}^{T-1} \frac{\delta n_i \delta n_{i+m}}{\bar{n}^2} = \frac{\langle \delta n_0 \delta n_m \rangle}{\bar{n}^2} \tag{24}$$

and

$$\mathrm{var}\, G(t) = \frac{1}{T^2}\mathrm{var}\left(\sum_{i=1}^{T} \frac{\delta n_i \delta n_{i+m}}{\bar{n}^2}\right) = \frac{1}{T\bar{n}^4}\mathrm{var}\,(\delta n_0 \delta n_m)\,. \tag{25}$$

There are two main sources for the fluctuations $\delta n(t)$ in the number of detected photons per sampling time. The first is the statistical nature of the system itself, i.e. fluctuations in the number N of fluorescent molecules in the sampling volume due to diffusion or chemical reactions. The relative fluctuation in photon counts $\sqrt{\mathrm{var}\,\delta n^{(1)}}/\bar{n}$ due to this source is related to the fluctuations in N: $\sqrt{\mathrm{var}\,\delta n^{(1)}}/\bar{n} = \sqrt{\mathrm{var}\,\delta N}/\bar{N} = 1/\sqrt{\bar{N}}$. These fluctuations contribute both to the signal $G(t)$ (as discussed above) and to the noise $\sqrt{\mathrm{var}\,(G(t))}$.

The second source of $\delta n(t)$ is the statistical nature of the photon emission and detection processes, i.e. the fluctuations in the number of detected photons per fluorescent molecule (shot noise). These fluctuations contribute to the noise only, since the fluctuations at different time intervals are not correlated. Shot noise depends on the total number $n(t)$ of detected photons and its relative value is $\sqrt{\mathrm{var}\,\delta n^{(2)}}/\bar{n} = \sqrt{\mathrm{var}\,\delta n}/\bar{n} = 1/\sqrt{\bar{n}} = 1/\sqrt{\nu\bar{N}}$, where ν is an average number of detected photons per molecule per sampling interval.

In most experimental situations and definitely in most of the situations where the FCS statistics is of concern, ν is small. For example, the typical diffusion time for a simple dye molecule in the FCS experiments is $\sim$100 μs. Then choosing a sampling time of $\sim$1 μs and taking the typical count rate of 40 000 photons per second per fluorescent molecule, we estimate $\nu \approx 0.04$.

For small values of ν and large $\bar{N}$, $\sqrt{\mathrm{var}\,\delta n^{(2)}}/\bar{n} \gg \sqrt{\mathrm{var}\,\delta n^{(1)}}/\bar{n}$ and the shot noise dominates the noise of the correlation function $\sqrt{\mathrm{var}\,(G\,(t))}$. Taking into account the fact that the shot noise is uncorrelated, we obtain from (25):

$$\mathrm{var}\,G\,(t) \approx \frac{1}{T\bar{n}^4}\mathrm{var}\left(\delta n_0^{(2)}\delta n_m^{(2)}\right) = \frac{1}{T\bar{n}^4}\left(\left\langle\left(\delta n_0^{(2)}\delta n_m^{(2)}\right)^2\right\rangle - \left\langle\delta n_0^{(2)}\delta n_m^{(2)}\right\rangle^2\right)$$
$$= \frac{1}{T\bar{n}^4}\left(\left\langle\left(\delta n_0^{(2)}\right)^2\right\rangle\left\langle\left(\delta n_m^{(2)}\right)^2\right\rangle - \left\langle\delta n_0^{(2)}\right\rangle^2\left\langle\delta n_m^{(2)}\right\rangle^2\right) = \frac{(\mathrm{var}(\delta n^{(2)}))^2}{T\bar{n}^4} = \frac{1}{T(\nu\bar{N})^2}.$$

Finally, the signal-to-noise ratio for the FCS measurement is

$$S/N = \frac{G\,(t)}{\sqrt{\mathrm{var}\,(G\,(t))}} \approx G\,(t)\,\nu\bar{N}\sqrt{T} \propto \nu\sqrt{T} \tag{26}$$

where we made use of $G\,(t) \propto 1/\bar{N}$.

We would like to point to the two main consequences of equation (26). First, as previously mentioned, for $\bar{N} \gg 1$ the statistics of FCS is independent of the number of molecules and depends only on the photon count rate per molecule and the total acquisition time. Second, the S/N dependence on ν is stronger than the dependence on T, which means that it is extremely important to optimize photon detection in the experiment: a 10-fold loss of detection efficiency has to be compensated for by a 100-fold increase in acquisition time.

The case of small $\bar{N}$ has been considered by Qian (1990) and Kask *et al* (1997). Below $\sim$10 molecules per sampling volume, the signal-to-noise ratio decreases monotonously with decreasing $\bar{N}$.

In addition, S/N might be limited by different imperfections of the experimental system, most notably by the background noise and by the correlated laser noise (Koppel 1974). Increasing the concentration of the molecules diminishes the contribution of the background in the overall signal. However, the concentration cannot be increased indefinitely, since the amplitude of the correlation function decreases with increasing $\bar{N}$ and at very high $\bar{N}$ the correlation function might be hidden in the correlated laser noise.

3. The modern realizations of experimental setups for FCS

In this section, we present the experimental implementation of FCS. First, we will introduce the standard setup of FCS since 1993, with the confocal geometry to optimize the collection of fluorescence. Then, we will review variations of the standard setup (with two-colour FCS, two-photon FCS and others) generating new possibilities of measurement. Finally, we will present a few practical considerations to help in the design of an FCS experiment.

3.1. The standard confocal illumination and detection scheme

As follows from the theoretical discussion, the FCS measurement requires small sampling volumes (to ensure a small number of molecules and, hence, a high amplitude of correlation function), as well as high photon detection efficiency and good rejection of background fluorescence. The renaissance in FCS is associated with the realization by Rigler *et al* (1993, 1992) that the confocal illumination scheme fits the above requirements perfectly.

In a confocal setup (figure 1(*A*)) the excitation laser light is directed by a dichroic mirror into a high-power objective, which focuses the light inside the sample. The fluorescence emission is collected through the same objective and focused onto a pinhole, so that the laser beam waist inside the sample is imaged onto the pinhole aperture. The conjugation of the objective and the pinhole creates a spatial filter, which efficiently cuts the sampling volume to

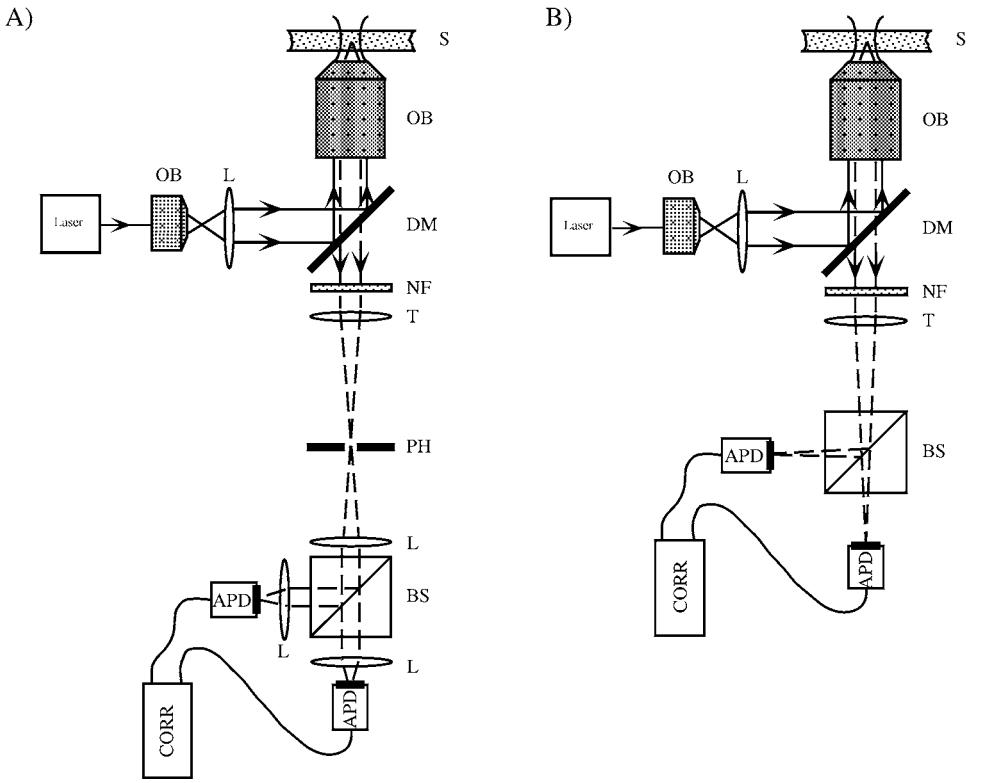

Figure 1. (*A*) Scheme of a standard confocal experimental setup for FCS. (*B*) Two-photon modification of the confocal setup. Abbreviations: S: sample; OB: objective; L: lens; DM: dichroic mirror; NF: notch filter; T: tube lens; PH: pinhole; BS: beamsplitter; APD: avalanche photodiode; CORR: correlator.

a diffraction limited size. After the pinhole, the fluorescence signal can be collected directly by a photon counting detector and processed into an autocorrelation function.

However, such a collection of emitted photons will yield a very distorted autocorrelation function for lag times shorter than 1 μs because of the 'afterpulsing' of the photon counting detectors. In any such device, there is a finite, albeit low, probability that a single detected photon will generate two electronic pulses (instead of one). This generates a spurious peak in the correlation function, associated with this very correlated detection noise. A simple solution to reduce the afterpulsing noise consists in splitting the collected light between two photodetectors and cross-correlating their outputs (figure 1(*A*)). In that case, the resulting cross-correlation function is formally similar to the autocorrelation function and is free from the afterpulsing noise.

Another point in collecting the fluorescence emission with two detectors is in the implementation of *two-colour* FCS (Schwille *et al* 1997). The principle of this technique is as follows: two interacting species are labelled with two different-colour fluorescent dyes and the optical filters are set in such a way that each of the photodetectors detects the fluorescence of either of the species. The cross-correlation function of the detectors' outputs is sensitive only to the correlated motion of the molecules of both components, i.e. to the motion of doubly labelled product resulting from the interaction of the two molecules. The amount of product can then be deduced from the amplitude of the cross-correlation function. Two-colour FCS is especially suited to studying the binding of different compounds to each other.

For two-colour FCS the light is split between the detectors by means of a dichroic mirror which separates the fluorescence emission of the two dyes from one another, and additional emission filters are set in front of the detectors in order to reduce the cross-talk between the detection channels. Still, since the emission wavelength ranges of the two dyes may not be perfectly separated, special care must be taken in analysing the data (Schwille *et al* 1997).

Typically, the two dyes have to be excited by two different laser lines. For that purpose, the laser is operated in a multi-line mode (Winkler *et al* 1999) or a second laser can be added to the setup (Schwille *et al* 1997). The alignment of the setup is somewhat more difficult in the latter case, as one has to make sure that the beams of both lasers are focused precisely in the same place in the sample.

3.2. Two-photon FCS and two-colour two-photon FCS

The invention of two-photon confocal microscopy by Denk *et al* (1990) inspired the use of the same optical scheme for fluorescent correlation spectroscopy (Berland *et al* 1995).

In the two-photon confocal setup (figure 1(*B*)) the high optical resolution is achieved through the use of non-linear two-photon absorption. The laser light is focused inside the sample with the help of a high power objective. As the probability of a two-photon event is extremely low, all of the absorption, and thereby fluorescent emission, occurs only in a small region near the focus where the energy density is the highest. Thus, as opposed to the single-photon scheme (figure 1(*A*)), in the two-photon setup the spatial filtering is an inherent property of the illumination path. There is no need in the pinhole to cut off background fluorescence and the emission light can be directly collected by the photon counting detectors.

As the probability of the two-photon event is proportional to the square of the intensity, the efficiency of excitation is greatly increased through an illumination in short pulses. Typically, femto- or pico-second infrared Ti–sapphire lasers are used.

As compared to the single-photon FCS, two-photon FCS is better suited for *in vivo* experiments (Schwille *et al* 1999a). First, the two-photon excitation (and therefore most of the photobleaching and photodamage detrimental to living cells) is restricted to the detection volume around the waist of the laser beam. Second, for the same dye, the excitation wavelength of the two-photon illumination is typically twice as long as that of the single-photon excitation, which greatly reduces the scattering of the excitation light in opaque biological tissues.

Despite the complexity (and the cost) of dealing with the pulsed infrared illumination, two-photon excitation might have some relative advantages for *in vitro* studies as well. The illumination and emission light are well separated in wavelengths and so the fluorescence light can be efficiently filtered from the scattered light in experiments. And, as pointed out by Heinze *et al* (2000), the two-photon excitation opens up new possibilities for two-colour FCS. The selection rules for two-photon excitation differ from those of single-photon excitation, so that some of the dyes with very different emission spectral characteristics might all be efficiently excited by the same two-photon illumination. This alleviates the need for precise alignment of two lasers in the two-colour FCS scheme.

3.3. Alternative schemes

In this section we briefly describe several variations of the standard FCS technique. For the most part these represent different enhancements or alternatives to the standard confocal setup.

3.3.1. Scanning FCS and image correlation spectroscopy. By the virtue of measuring the fluctuations of the number of particles in the detection volume, standard FCS is mostly sensitive

to the fast moving molecules and relatively insensitive to the immobile or slowly moving aggregates (e.g. protein clusters in the cell membrane). The latter case can be helped by scanning the sample through the laser beam or by scanning the laser beam across the sample (Petersen 1986, Petersen *et al* 1986, Berland *et al* 1996). As fluorescent aggregates are passing through the detection volume, the intensity of emission fluctuates. And, just as in standard FCS, the number of fluorescent particles can be deduced from the amplitude of the correlation function of intensity fluctuations in the scanning FCS.

The same idea is used in image correlation spectroscopy (Petersen *et al* 1993, Huang and Thompson 1996, Srivastava and Petersen 1998, Wiseman and Petersen 1999), where the correlation in space domain substitutes for the correlation in time.

3.3.2. Time-gated FCS. Time-gated FCS (Lamb *et al* 2000) is an enhancement of the standard FCS technique, capitalizing on the fact that different fluorescent dyes have different excited-state lifetime distributions and/or can change them upon binding to other molecules. Then by using pulsed illumination and by selectively suppressing photon counting after the laser pulse, the contribution of the relevant species to the correlation function can be enhanced.

3.3.3. Total internal reflection (TIR) scheme. In TIR the evanescent wave penetrating into the media of lower optical density decays exponentially with distance from the interface. This made TIR the natural candidate for creating the optically restricted excitation illumination in some of the early FCS setups (Thompson *et al* 1981, Thompson and Axelrod 1983). Although TIR has not been implemented in recent FCS experiments, it offers some promise in the study of chemical reactions on interfaces.

3.3.4. X-ray FCS and Raman correlation spectroscopy. A recent proof-of-principles study showed that the FCS technique can be extended into the x-ray domain (Wang *et al* 1998). Wang *et al* (1998) used synchrotron radiation to excite x-ray fluorescence of gold and ferromagnetic colloidal particles. This technique was used to monitor the diffusion and sedimentation of the colloidal particles.

The principle underlying FCS can be applied as well to study the dynamics of the systems by means of Raman scattering (Schrof *et al* 1998). Like the fluorescence spectrum, the Raman scattering spectrum is specific to the chemical structure of the compounds. Schrof *et al* (1998) showed the feasibility of Raman correlation spectroscopy, i.e. that the autocorrelation function of Raman scattered light from the colloidal beads can be collected to study their diffusion. Two-colour Raman correlation spectroscopy analogous to two-colou FCS is also possible (Schrof *et al* 1998). Raman scattering is much weaker than fluorescence, which limits its usefulness in correlation spectroscopy applications. However, it has at least one advantage as compared to fluorescence: unlike fluorescence, Raman scattering cannot be bleached.

3.4. Practical considerations

We would like to present here a few practical considerations for setting up an FCS experiment. This section sums practical issues, taken from technical papers as well as from our personal experience in implementing FCS.

3.4.1. The choice of dyes. An FCS measurement relies on the fluorescence of the compound under study, this fluorescence being either natural (as for the green fluorescent protein (GFP), see section 4), or, more generally, resulting from specific dye-labeling of the compound

of interest. While there is a huge variety of dyes commercially available for fluorescence microscopy, not all of these dyes would perform well in an FCS experiment.

The discussion of the statistics of FCS (section 2.5) shows that it is the fluorescence emission per molecule that determines the quality of the measurement. Thus, the dye has to be bright, i.e. it must be characterized by high extinction coefficient and high quantum yield.

Next, different deficiencies of the dyes must be avoided. The fluorescence emission is proportional to the excitation at low laser intensities only. At high intensities the dye emission saturates because of two reasons. First, the emission of the dye is limited to one photon per residency in the excited state (whose lifetime is typically in the range of few nanoseconds). Thus, it cannot be better than 10^8 photons s^{-1}. Second, even before reaching this limit, the fluorescence of the dye saturates because of trapping in a non-fluorescent triplet state (see section 4.2). The triplet state not only limits the emission, but also shows up in the correlation function in the microsecond range concealing other processes which might be occurring with the labeled molecule in this time range.

Finally, upon prolonged illumination the dyes can be bleached irreversibly. While normally this is not a problem for FCS measurements on mobile molecules (their diffusion time across the sampling volume is short, typically 100 μs–1 ms, compared to the bleaching time), the photobleaching is of concern for the experiments on immobile or slowly moving objects.

To sum up, the dyes for the FCS experiment should be characterized by high extinction coefficient, high fluorescence quantum yield, low singlet-to-triplet state quantum yield and low photobleaching. Currently the dyes which comply best with these requirements are the derivatives of rhodamine: tetramethylrhodamine (TMR) and carboxyrhodamine (Rh6G). These dyes are available commercially with numerous bioconjugation active groups. So, if other experimental conditions are not imposing a different choice, it is advisable to use TMR or Rh6G for labelling purposes. However, other fluorescent dyes have been successfully used as well. Also one should remember that the photodynamical properties of a dye might change upon binding to the 'host' molecule.

3.4.2. Lasers. Most of the commercial dyes are optimized for the spectral lines of argon, argon–krypton or helium–neon lasers, so, once the laser is chosen, there should be no problem in finding an appropriate dye and vice versa.

Special care must be taken in defining the laser excitation in confocal FCS. The laser beam should be expanded but should not overfill the rear pupil of the microscope objective, to define the smallest confocal volume. The intensity of the excitation laser light should be low enough, so that the dye emission is in the linear range of its dependence on excitation (typically a few tens of microwatts). At higher intensities the detection volume appears to increase as the emission of the dye molecules in the centre of the confocal volume saturates and, therefore, the relative contribution of the molecules at the periphery increases. This effect must be taken into account and calibrated when performing experiments with dyes of different saturation limit.

3.4.3. Microscope objectives. For the best collection of fluorescence, high power objectives are used. Oil-immersion objectives are characterized by the highest numerical aperture (NA $\sim$ 1.4). However, they are designed to focus and collect light in a high refractive index environment (that of the immersion oil or of the cover glass), such that their optical quality is reliable only when the focal plane is right at the surface of the cover glass. Focusing the laser excitation deeper inside aqueous samples (typically more than a few microns from the glass–water interface) generates optical aberrations as well as sub-optimal fluorescence

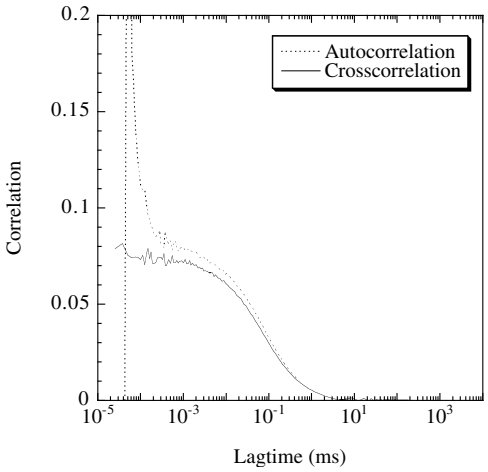

Figure 2. Comparison of the autocorrelation and the cross-correlation of the collected fluorescence of freely diffusing Rh6G. Note the peak at 100 ns in the autocorrelation function, due to the afterpulsing of the detector.

collection, which can jeopardize the quality of an FCS measurement. This problem, well known in confocal microscopy, is solved through the use of water-immersion objectives. Although the numerical aperture of these objectives (NA $\sim$ 1.2) is smaller than that of the oil-immersion ones, for experiments with aqueous samples, water-immersion objectives have a clear advantage of focusing the excitation light and collecting the emission efficiently.

3.4.4. Pinholes. The optimization of the pinhole size was considered by Rigler *et al* (1993) both theoretically and experimentally. The best signal to backround values were obtained with pinholes of the size of the image of the laser beam waist in the plane of the pinhole. Typically the pinhole diameter should be about 30–50 μm, depending on the objective. However, larger pinholes up to 250 μm were used as well in the studies where large detection volumes were needed (Börsch *et al* 1998, Eggeling *et al* 1998).

As an alternative to the pinhole, an optical fibre can be used to define the detection volume and feed light to the photodetector (Haupts *et al* 1998, Schwille *et al* 1999b, Heikal *et al* 2000).

3.4.5. Detectors. In FCS, it is absolutely essential to use detectors with high quantum efficiency (QE). In this respect avalanche photon detectors (APD) with QE $\sim$ 70% at 560 nm (from Perkin–Elmer—former EG&G optoelectronics division) appear to be unsurpassed. Since photomultiplier tubes typically have a quantum efficiency of less than 20% and even less in the green and red regions of the spectrum where many of the popular dyes emit light, they are presently rarely used in FCS. However, future technical improvements might make photomultiplier tubes more efficient (for example, Hamamatsu Photonics introduced recently new photomultiplier tubes based on a GaAs photocathode with QE $\sim$ 30% in the green region of the spectrum).

As we have already mentioned, all of the photon counting devices (photomultipliers as well as APD) have a problem of 'afterpulsing', which can be efficiently dealt with by splitting the light between two detectors. We illustrate this problem in figure 2 where the autocorrelation function of a fluorescence emission collected by a single detector is compared to the cross-correlation of the output of two detectors. A strong peak, characteristic of afterpulsing, distorts the autocorrelation function below 100 ns, and up to 1 ms, but not the cross-correlation. Although this distortion is weak at 1 ms, it perturbs the flatness of the correlation function at small time scales, and forbids a correct estimation of the amplitude of the correlation function.

3.4.6. Correlator. Unlike the first correlators (set in linear scale), most of the correlators today have their delay channels spaced on a logarithmic ladder, so that the correlation function is presented as a function of the logarithm of the lag time (see, e.g., figure 2). This displays the correlation function at all time scales in a single measurement. This is especially convenient in the FCS experiments where the diffusion term (equations (18) and (23)) slowly decays over many time scales.

3.4.7. Analysis. Many pitfalls are to be avoided in the analysis of an FCS measurement. Although some considerations of the statistical analysis presented here might not be specific to FCS, they are of crucial relevance to the accuracy of the FCS technique.

The correlation function picks up every process that causes fluctuations in the collected light intensity. Moreover, processes overlapping in time scales, even if independent, do not simply add up in the correlation function, but might be interconvolved in a complicated manner. This just stresses the necessity to eliminate all of the irrelevant processes from the experimental system.

One of the phenomena causing distortion of the correlation function is the triplet state formation (unless of course it is itself the subject of the investigation). Although hard to eliminate completely, the distortion can be reduced through the choice of better dyes and lower excitation intensity.

If it is impossible to eliminate the non-relevant processes from the system, they should be measured in independent control experiments. One thing which we would not recommend (but which is frequently used nevertheless) is a direct fit of a correlation curve with a single function incorporating too many fitting parameters related to too many phenomena. The statistical robustness of this kind of fit is hard to estimate and thus is questionable.

Finally, rare but brightly fluorescent events (like the passage of large agglomerates of labelled molecules through the detection volume) might cause distortion of the correlation function. From our experience, it is preferable to accumulate the correlation function in many short runs instead of a single long run. Then these runs can be individually checked for unusually big spikes of intensity and/or inaccurate baselines of the correlation function, and discarded if needed. Accumulation of many runs also allows us to estimate the statistical error of every data point to be used in the fitting procedures as weight parameters (errors will be different for different channels due to the logarithmic layout).

In conclusion, although confocal FCS can be readily implemented with commercial setups, the possible sources of artefacts in the correlation function must be understood before carrying out a measurement.

4. The experimental studies with FCS

4.1. Brief description of the biophysical systems studied in FCS

As most of the experiments described in this review deal with biomolecules, we would like to introduce briefly the relevant biological systems and their associated problematics. In particular, as most of the biomolecules are not naturally fluorescent, we would like to present recent progress in bioconjugation chemistry to specifically tag biomolecules with fluorescent dyes, for further study by FCS.

4.1.1. Lipid vesicles. Lipids are amphiphilic molecules which in aqueous solutions self-assemble into floppy 2D membranes—bilayers, whereby the hydrophilic heads of the molecules are exposed to the solution while the hydrophobic tails are hidden within the bilayer.

A bilayer may close onto itself to form a vesicle: a structure with an internal compartment bounded by the membrane. Lipid vesicles are model systems of cell plasma membranes (PM), whose structure and dynamics are of special interest to cell biology. In particular, the lipid phase segregation within a vesicle's bilayer is of utmost relevance to the understanding of the activity of membrane-associated enzymes.

The introduction of fluorescent tags on lipid vesicles can be done by direct derivatization of the lipid building block (Hermansson 1996), or by intercalation of hydrophobic dyes into the bilayer, or by coupling dye and lipid molecules through the strong biotin–streptavidin linking (which is borrowed from the living world). When the biomolecule of interest is a membrane protein, one can also tag the proteins before intercalating them within the lipid bilayer.

4.1.2. Nucleic acids (DNA and RNA). Deoxyribonucleic acids are the molecules of choice in many FCS experiments. Their polymeric structures, associated with the combinatorial diversity of their base composition, make them the ideal system to study biomolecular folding, structure/function relationships and molecular recognition. The base complementarity discovered by Watson and Crick (adenosines pair with thymidines, cytosines pair with guanosines) imposes a simple rule to the self-assembly of DNA molecules. DNA also constitutes a fascinating physical system, exhibiting a variety of physical phenomena from polymer-like random-coil fluctuations to melting–hybridization phase transition (separation and re-annealing of two complementary DNA strands at elevated temperatures or in denaturating chemical conditions).

The bioconjugation chemistry of DNA has been greatly simplified in the 1990s to serve genomic research's advancement (Hermansson 1996, Cantor and Smith 1999). Solid-phase chemistry allows the complete synthesis of oligonucleotides of any specific sequence, up to 100 bases. Since DNA by itself is rather inert chemically, in order to couple the fluorescent dyes one must introduce chemically active modifications into DNA at specific locations. Today, most modifications of DNA molecules are achieved during the solid-phase synthesis. Unspecific labelling of double-stranded DNA molecules is also possible through the use of intercalating dyes (e.g. ethidium bromide). These dyes insert themselves into the double-helical structure where they become strongly fluorescent. Long DNA molecules (up to several millions of base pairs) can also be prepared routinely by purification from biological sources (viruses, plasmids, etc) or by synthetic preparation with the polymerase chain reaction.

Let us point out that, because of its monodispersity, DNA is often the dream molecular system in polymer physics research. A lot of FCS studies have used DNA molecules as an easy-to-use benchmark for further developments. For example, many binding assays (see references in section 4.4) have been designed and optimized with two complementary oligonucleotides, whose binding/debinding is associated with fluorescence fluctuations to be monitored by FCS.

From the biological point of view, RNA molecules are even more interesting systems to study than DNA, because of their enzymatic activities, such as self-splicing, or nucleic acid ligation. However, their lack of chemical stability as well as the complication of the bioconjugation protocols have limited their use in FCS experiments.

4.1.3. Proteins. FCS has also been used to study the dynamics of proteins' conformational fluctuations, as well as their interaction with other biomolecules. Designing a fluorescence change in a protein or in its substrate associated with a specific molecular event is the critical step before implementing FCS. Experimenters are usually guided by their knowledge of the crystal structure of the protein of interest. However, the specific bioconjugation of artificial dyes is more difficult for a protein than for DNA (chemically active amino acids cysteines and lysines often exist in multiple copies in a protein) and requires the engineering of the protein's sequence.

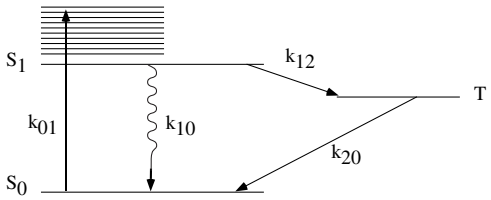

Figure 3. Jablónski diagram for photochemistry. This simplified diagram with three relevant states accounts for the fluorescence fluctuations of Rh6G, as measured by FCS (S_0: ground state (singlet), S_1 singlet excited state and T: triplet state). The lifetime of the triplet state is so long (e.g. 1 μs) that its occupation becomes limiting towards further fluorescence excitation ($S_0 \rightarrow S_1$) and the state acts like a dark state.

Contrary to lipids and nucleic acids, there exists a protein of robust natural fluorescence: the GFP. GFP of the jellyfish *Aequorea victoria* has been cloned in 1995, and has revolutionized biology since (Tsien 1998). GFP is a relatively small protein whose gene can be fused to any protein's gene of interest. The cellular machinery transcribes the DNA code for the target protein in concatenation with the code for GFP, and generates a fluorescently labelled protein. The resulting construct is a fusion protein, with the biochemical properties of the target protein and the fluorescence of the GFP. Bioconjugation as well as purification becomes obsolete when using GFP as a fluorescent tag, enabling direct tracking of GFP-fused proteins in living cells. Variants of GFP with different spectral properties (blue, cyan or yellow GFP) are available today.

4.2. Photodynamical properties of fluorescent dyes

As mentioned in section 3.4, fluorescent dyes possess non-trivial photodynamic properties which leave footprints in the autocorrelation function of the fluorescent emission. While this normally constitutes a source of undesirable noise in experiments with dye-labelled biomolecules, these footprints provide a convenient way to study the photophysical properties of the dyes themselves. The information obtained in these measurements can be useful in choosing the most appropriate dye for labelling purposes.

We will present three examples of applications of FCS in photophysics: the determination of the kinetics of triplet state formation, of photon anti-bunching and of photobleaching processes.

4.2.1. Triplet state kinetics. To achieve single-molecule detection of fluorophores, one must ensure a high fluorescence emission of dyes, which itself requires a high turnover between the excited singlet state S_1 (pumped by the excitation photons) and the ground singlet state S_0 (see diagram in figure 3). The rate k_{01} of $S_0 \rightarrow S_1$ transition is controlled by the pumping light intensity I: $k_{10} = \sigma I$, where σ is the photon absorption cross section. The rate k_{10} of the relaxation $S_1 \rightarrow S_0$ (associated with fluorescence photon emission) is the inverse of the excited state's lifetime (typically a few nanoseconds in water for fluorescein) and becomes limiting to the overall turnover rate at high pumping intensities. Thus, under strong pumping (above typically a few kW cm^{-2}), the excited singlet state S_1 becomes highly populated. In these conditions the transition from the excited singlet state S_1 to the lowest triplet state T becomes probable, followed by relaxation into the ground state S_0 (figure 3).

Forbidden by quantum symmetry rules, singlet–triplet and triplet–singlet transitions are non-radiative and slower (i.e. with smaller respective rates k_{12} and k_{20}) than the singlet–singlet transition.

In the complete description of this system (Widengren *et al* 1995), there are three photochemical species, and thus three modes of chemical fluctuations. The first one corresponds to the conservation of matter and is characterized by a null rate. The second one corresponds to the single–singlet relaxation and is thus characterized by a large rate (larger than the inverse lifetime of S_1): we will consider this mode of relaxation in the next section. The third one, the slowest mode, involves the singlet–triplet transition, to be discussed in this section.

The description of singlet–triplet transition kinetics can be simplified by taking into account that it is non-radiative and slower than the singlet–singlet transitions. Then for FCS purposes, the dye is fluctuating between a light-emitting state (the singlet states) and a dark state (the triplet state). Thus, the photodynamics of the dye can be schematically characterized by a simple chemical reaction:

$$\text{Fluorescent } (S_0, S_1) \underset{k_{20}}{\overset{k_{12} P_{S_1}}{\rightleftarrows}} T \text{ Non-fluorescent}$$

where the forward rate k_{12} has been normalized by the fraction P_{S_1} of molecules occupying the excited state S_1 among molecules in the single state (this normalization quantitatively takes into account the fact that the transition into the triplet state is possible only from S_1 and not from S_0).

Thus the description of the triplet state kinetics is similar to the description of the isomerization transition between fluorescent and non-fluorescent states (see section 2.4). In a simplified treatment, the expression for the correlation function for the present case is then equivalent to equation (23):

$$G(t) = \frac{1}{\bar{N}} \left(1 + \frac{t}{\tau_D}\right)^{-1} \left(1 + \frac{t}{\omega^2 \tau_D}\right)^{-1/2} \left(1 + \frac{p}{1-p} \exp\left(-\frac{t}{\tau}\right)\right)$$

where p is the fraction of dye molecules in the triplet state. As in the isomerization case, the relaxation time τ is determined by the sum of forward and backward transition rates: $1/\tau = k_{12} P_{S_1} + k_{20}$. As $k_{01}, k_{10} \gg k_{12}, k_{20}$, we can estimate P_{S_1} from the equilibrium of the $S_0 \leftrightarrow S_1$ reaction: $P_{S_1} = k_{01}/(k_{01} + k_{01})$. Then

$$\frac{1}{\tau} = k_{20} + \frac{k_{12} k_{01}}{k_{01} + k_{10}} = k_{20} + \frac{k_{12} \sigma I}{\sigma I + k_{10}}.$$

At low intensity, the relaxation of this mode is determined by the triplet to ground singlet transition, with a rate k_{20}. At high laser intensity, the excited-singlet-to-triplet transition becomes significant and the relaxation rate is $(k_{20} + k_{12})$. By varying the intensity the characteristic transition rates k_{20} and k_{12} can be determined.

In contrast to the isomerization rates, the rate of the triplet state formation depends on excitation intensity (through P_{S_1}). A more detailed analysis than the one presented here (Widengren *et al* 1995) takes into account the spatial distribution of the singlet-to-triplet probabilities resulting from the non-uniform illumination in the confocal volume.

FCS has been used as a spectroscopy tool to characterize the kinetics of triplet state formation in organic dyes (Widengren *et al* 1995, 1997) or GFP (Haupts *et al* 1998, Widengren *et al* 1999a, 1999b). The transition rates k_{20} and k_{12} are typically in the 1–10 μs^{-1} range and depend on the dyes and on the solvents used.

Note that there is no 'direct' fluorescence signature associated with the triplet state formation i.e. the relaxation from triplet back to the ground level does not need to be radiative to be detectable by FCS.

4.2.2. Antibunching. When dealing with the photodynamics of triplet state formation, we essentially ignored the transitions between the ground and excited singlet states (S_0 and S_1) by grouping them together into a single state. This is justified as the characteristic time scales of singlet–triplet transitions ($\sim$1 μs) exceed those of singlet–singlet transitions ($\sim$10 ns) by at least two orders of magnitude. However, when focusing on the nanosecond time range, the contribution of the $S_0 \leftrightarrow S_1$ transitions to the correlation function has to be considered. This contribution has a character of *anti*-correlation, a phenomenon of purely quantum nature stemming from the fact that the emission of a photon is a result of the *transition* $S_1 \rightarrow S_0$ between the states (compare to the treatment of, e.g., isomerization, where the fluorescence is associated with a state by itself). Having emitted a photon, in order to emit another photon the dye molecule has to undergo the complete turnover from the ground to the excited state and then back to the ground state. The rate of this turnover is determined by the excitation rate and by the lifetime of the excited state, and before the turnover is complete no photon is emitted. Thus for any given molecule there is a certain 'dead' time after the emission of a photon during which the probability of emitting another photon is extremely low. This effect is called anti-bunching and it results in the anti-correlation in the FCS correlation curve.

Mets *et al* (1997) have used FCS to measure the anti-bunching time of Rhodamine 6G in water. The FCS technique, with its continuous wave excitation, is an alternative to the standard measurement by pulse excitation with a mode-locked laser. However, the FCS setup has to be modified to include a time-to-amplitude converter and a multichannel pulse-height analyser to achieve faster electronics. To circumvent the dead time and the afterpulsing of the photodetectors, Mets *et al* (1997) also split the emitted light between two detectors and cross-correlated their outputs (see section 3).

A simplified analysis of anti-bunching leads to the following expression for the FCS correlation function:

$$G(t) = \frac{1}{\bar{N}} \left(1 - \exp\left(-\left(k_{10} + k_{01}\right) t\right)\right)$$

where, like in the previous subsection, $k_{01} = \sigma I$ and k_{10} are the excitation and decay rates, respectively. Note that translational motion and triplet state depletion can be neglected as they are irrelevant to the time channels under study (here from 1 to 15 ns).

A more detailed treatment of the experimental situation takes into account the non-uniform distribution of illumination (Mets *et al* 1997). The photodynamical properties of Rh6G dyes can be deduced from the relaxation of FCS correlation function at different excitation intensities. Mets *et al* (1997) characterize Rh6G fluorescence with a decay rate $k_{10} = 2.57 \times 10^8\ \mathrm{s}^{-1}$, i.e. a lifetime of 3.89 ns for the singlet excited state and an excitation cross section of $\sigma = 0.9 \times 10^{-16}\ \mathrm{cm}^2$. These values compare fairly well with the values measured by other methods. The excitation cross section appears to be underestimated by a factor of 2, which is explained in terms of the wavefront distortion of the excitation light in a sharply focused confocal illumination beam.

4.2.3. Photobleaching. Fluorescent dyes in their excited state have a certain probability to undergo irreversible destruction (a process named photobleaching). For weak illumination, this probability is independent of the excitation intensity. This means that, irrespective of the excitation, for each dye there is a characteristic number of photons emitted before the dye undergoes photobleaching. However, for high illumination intensities the picture is more complicated and involves photobleaching kinetics from a number of excited states (Eggeling *et al* 1998). This photobleaching phenomenon can be of concern in FCS as well as single-molecule spectroscopy, whereby one tries to maximize the fluorescence emission of individual dyes.

Eggeling *et al* (1998) characterize the photobleaching kinetics with the help of FCS. Although photobleaching is a non-equilibrium process, since the confocal volume is small relative to the overall volume of the sample, the situation in the sampling volume can be considered as quasi-equilibrium and the FCS technique can be applied.

In conclusion, FCS can be an easy-to-implement alternative to more classical spectroscopy techniques (such as time-gated fluorescence detection) to measure the photochemical properties of dyes (triplet state lifetime, excited-state lifetime or photobleaching kinetics).

4.3. Study of translational and rotational diffusion with FCS

4.3.1. Translational diffusion. The translational diffusion of biomolecules has classically been assessed equivalently by FCS or FRAP. However, there are at least two advantages in using FCS: first, it is a non-invasive technique (Fahey and Webb 1978), where photobleaching is minimized (whereas FRAP generates chemical radicals of high toxicity for a living cell); second, it requires a smaller quantity of fluorophores per field of view, implying less disruption of a biomolecular environment (Korlach *et al* 1999).

The measurement of translational diffusion is probably the simplest measurement which can be performed with FCS: the molecules of interest are labelled with a fluorescent dye, their motion in the sampling volume results in the correlation function of the types of (18) or (19) with the characteristic relaxation times related to the diffusion time scale across the sampling volume.

In this section we illustrate this type of application of FCS with measurements of the mobility of biomolecules within lipid bilayers.

The fluidity of the lipid molecular bilayer is an important concept of cell biology. It allows the transversal motion of lipids and inserted proteins to control the transduction of intracellular and extracellular responses. In fact, the structure of the cell membrane is very dynamic, with possible segregation (or phase separation) of its constituents (lipids or proteins).

The techniques of FCS (Fahey *et al* 1975) and FRAP (Schlessinger *et al* 1975) were simultaneously applied to measure the translational diffusion of the lipid-intercalating dye 3,3-diocadecylindocarbocyanine iodide (DiI) within lipid bilayers. Typical translational diffusion coefficients of DiI are 9×10^{-9} cm^2 s^{-1} in cell membrane and 3×10^{-7} cm^2 s^{-1} in artificial lipid bilayers. These diffusion coefficients were shown to be weakly affected by temperature or by solvent content. However, for the lipid bilayer composed of dilauroyl phosphatidylcholine (DLPC) or dimyristoyl phosphatidylcholine (DMPC), DiI diffusion coefficient within the bilayers collapses from 10^{-8} cm^2 s^{-1} to less than 10^{-10} cm^2 s^{-1}, at 23 °C for DLPC and 42 °C for DMPC (Fahey and Webb 1978). This jump in the fluorescent probe diffusion coefficient, measured by FCS or FRAP, is consistent with a phase transition in the lipid organization within these artificial bilayers from gel-like (at high temperature) to liquid crystalline (at low temperature).

These phase transitions had already been documented in the 1970s by NMR with spin-probe labelled lipids. However, FCS and FRAP provide a potential for a spatially resolved measurement of the coefficient of diffusion, which becomes crucial to characterize lipid bilayers in which different structural phases coexist.

For example, recent work by Korlach *et al* (1999) has unravelled the coexistence of three lipid phases in giant unilamellar vesicles by confocal FCS. The vesicles under study were composed of a mixture of DPPC, DMPC and cholesterol. The fluorescent DiI is intercalated as a probe of lipid self-diffusion. FCS measures three values for its translational coefficient of diffusion: 3×10^{-8} cm^2 s^{-1} in a fluid phase, 2×10^{-9} cm^2 s^{-1} in a high cholesterol content phase and 2×10^{-10} cm^2 s^{-1} in a spatially ordered phase. The resolution of the confocal FCS

technique enabled Korlach *et al* (1999) to confirm the coexistence of these three lipid phases on the same vesicle.

4.3.2. Rotational diffusion. The probability of light excitation of a dye molecule depends on the angle between its excitation dipole moment and the polarization vector of exciting light. Thus, if a dye is freely rotating, its excitation rate and therefore its emission are fluctuating. These fluctuations contribute to the FCS correlation function a term with the characteristic time scale of rotational diffusion (Ehrenberg and Rigler 1974, Aragón and Pecora 1975): $\tau_{\text{rotation}} = \pi\eta l^3/(k_{\text{B}}T)$, where η is the buffer viscosity, k_{B} is the Boltzmann constant and T is the absolute temperature.

In most applications, it is difficult to detect the rotational diffusion time, as it is small and comparable to the anti-bunching time (at 1–10 ns), the dead time of the detector (at 10–30 ns), or the triplet relaxation time (at 0.1–1 μs). In the case of bulky molecules and aggregates with rigidly attached fluorophores, the rotational diffusion time becomes accessible to the FCS measurement. For example, Rigler *et al* (1992) reported measuring a rotational diffusion time of 16 μs for an acetylcholine receptor, tagged with Rh6G-coupled α-bungarotoxin. This rotational diffusion is too slow for this protein of molecular weight 290 kDa, and Rigler *et al* (1992) mention the possible formation of aggregates as an explanation of the discrepancy.

A rotational diffusion of GFP has also been reported by Widengren *et al* (1999a). The characteristic rotational time is around 20 ns, consistent with a molecular size of $l \approx 3$ nm for GFP.

Classically, rotational diffusion is detected with the anisotropy decay of the emitted fluorescence excited from a linearly polarized source. However, this technique is limited to fluorescent objects whose excited-state lifetime is comparable to the rotational diffusion time. In FCS, there is no such limitation, and rotational diffusion of bulky molecules is measured without invoking phosphorescent groups (with long excited-state lifetime).

The second advantage of FCS compared to the fluorescence anisotropy decay technique is the robustness of the measurement. The rotational diffusion relaxation has a well-defined time signature in the autocorrelation function. This is independent of the non-correlated background fluorescence, which affects fluorescence anisotropy measurements. FCS gives an absolute measure of the rotational diffusion time, and thus an absolute measure of the molecular size of the molecule of interest.

Finally, one must notice that measuring the rotational diffusion constant is not necessarily redundant with a measurement of the translational diffusion constant, as they assess molecular mobilities at different spatial scales. For freely diffusing molecules, both diffusion time scales are determined by the radius of the molecule and the viscosity of the buffer. The rotational diffusion time can be computed as a time scale of diffusion on its own scale (hence the dependence on the cube of the radius of the molecule), while the translational diffusion time is linear with the radius of the molecule. However, for molecules undergoing confined diffusion, the translational diffusion is limited by obstacles, while the rotational diffusion remains essentially free. Thus, FCS can offer, in a single measurement, an evaluation of the molecular size of the fluorescent molecules as well as the typical size of its diffusion confinement.

4.4. FCS as a binding assay

The most frequent application of FCS consists in assaying molecular interactions (binding/debinding). The method is best suited to study the binding of a small compound (e.g. a ligand) to a bigger molecular object (the ligand's receptor). Indeed, if the small compound

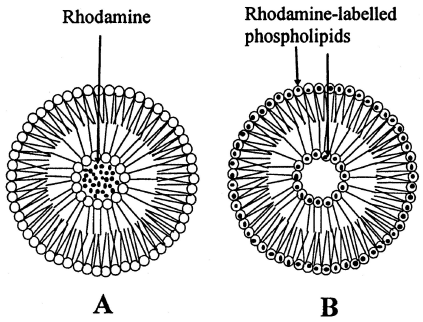

Figure 4. Schematic presentation of the cross section of vesicles from Pramanik *et al* (2000) (copyright 2000, with permission from Elsevier Science). (*A*) Vesicles made from phospholipids together with added rhodamine where rhodamine is entrapped inside (REV). (*B*) Vesicles made from rhodamine-labelled phospholipids (RLV). In RLV rhodamine is covalently bound to the head groups of phospholipids. Thus, rhodamine is not trapped inside RLV, i.e. the inside of RLV is free of dye molecules.

is labelled with a fluorescent marker, FCS can monitor its binding onto the large object as a slowdown in diffusion. When the chemical kinetics of binding/debinding is much slower than the diffusion kinetics of the molecules across the sampling volume, two main contributions can be resolved in the correlation function: the first one from the fast diffusion of a free small compound and the second one from the slow diffusion of the complex. By analysing the correlation curve it is possible to measure the concentrations of both the unbound and bound fractions (see equation (20)). The best results are obtained if the aspect ratio of the confocal volume (ω), the diffusion time scales (τ_{Di}) and the fluorescence per molecule (Q) for both the small compound and the complex are measured in separate experiments. Then the contribution of each species to the FCS correlation function can be reliably deconvolved in the mixture (Meseth *et al* 1999).

A number of different studies have been performed with this method: hybridization of DNA strands to each other (Kinjo and Rigler 1995, Auer *et al* 1998, Björling *et al* 1998) and to RNA (Schwille *et al* 1996), binding of ligands to their receptors (Auer *et al* 1998, Börsch *et al* 1998, Craenenbroeck and Engelborghs 1999, Schüler *et al* 1999, Wohland *et al* 1999, Schürer *et al* 2001), to other proteins (Meyer-Almes *et al* 1998, Häsler *et al* 1999, Pack *et al* 1999) and binding of proteins to lipid vesicles (Dorn *et al* 1998, Takakuwa *et al* 1999) have all been analysed.

In particular, in a rather original application of this technique Pramanik *et al* (2000) study the effect of the small peptides melittin and mangainin on lipid vesicles. They prepare two kinds of vesicles to address the issue whether these peptides poke holes in lipid vesicles or break down the lipid bilayers (figure 4): the first type of vesicles entrap in their interior a solution of rhodamine dye molecules (rhodamine-entrapped vesicles, REV) whereas the second type of vesicles is made of lipids chemically labelled with rhodamine (rhodamine-labelled vesicles, RLV). The diffusion of rhodamine is slow when they are vesicle-bound (the diffusion coefficient is that of a 40 nm vesicle), and fast when the dye is free in solution (the diffusion coefficient corresponds to a molecular dimension of 1.5 nm).

Pramanik *et al* (2000) show that melittin does not affect the FCS correlation function measured on RLV, which proves that the vesicles are not broken into parts by melittin and stay the same in size and in number. Yet the correlation function of REV upon introduction of melittin changes dramatically: the number of moving objects rises (the amplitude of the correlation function decreases) about fivefold and the characteristic diffusion time approaches that of free rhodamine. Thus, rhodamine from the interior of the vesicles is released into

solution. Assuming that the interaction of melittin with RLV and REV is similar, i.e. the RLV vesicles are not broken, Pramanik *et al* (2000) conclude that melittin makes channels in the vesicle membrane that do not destroy the vesicle as a whole but permit the rhodamine molecules to escape from the interior of the vesicle.

As opposed to melittin, the introduction of mangainin affects the correlation functions of both REV and RLV in a similar manner: the number of moving objects rises and the diffusion time decreases to match that of rhodamine molecules. From this result Pramanik *et al* (2000) conclude that mangainin destroys the vesicles into single lipids.

This implementation of FCS to study these interactions of peptides with lipid vesicles is above all elegant, as the system has been designed to generate a robust diffusion change for the labelling dyes upon interaction.

It is clear that the feasibility of the measurement of binding through the change in diffusion coefficient depends critically on the difference in the sizes of the interacting components. Meseth *et al* (1999) have analysed the sensitivity of this kind of measurement. They show that the FCS measurement of a binding reaction is not reliable if the ratio of diffusion coefficients of the labelled species and of the bound complex is smaller than a certain factor, which depends on the fluorescence yield and the relative fractions of compounds and which is generally in the range from 1.6–10. In those cases where the difference in diffusion coefficients between bound and unbound species is not large enough, the measurement of binding can be done through the implementation of two-colour FCS (Schwille *et al* 1997). The basic principle of this method has been outlined in the instrumentation section (see section 3.1): each of the two interacting compounds has to be labelled with a different fluorophore, such that the fluorescence of each species can be acquired with a separate detector. The cross-correlation of the two detectors' signals will essentially monitor the correlated diffusion of molecules bound into a complex. The amplitude of the cross-correlation function is then the inverse of the absolute number of complexes in the field of view. Thus, the binding kinetics can be monitored by two-colour FCS when it is sufficiently slow compared to the time of accumulation of the cross-correlation function (Schwille *et al* 1997).

Although the principle of this measurement is very elegant, its experimental implementation is somewhat more cumbersome than the standard single-colour FCS. First, the crosstalk between the two detectors has to be calibrated: the spectrum of the dyes' fluorescence is typically rather broad, so that in fact each detector has a fluorescence contribution from each of the dyes. With the proper choice of dyes and filters, though, the cross-talk contribution to the correlation function can be made negligible. Second, in general, the two dyes have to be excited by different lasers. Then special care must be taken about the alignment of the setup to make sure that the confocal volumes defined by both lasers perfectly coincide. Schwille *et al* (1997) have suggested a nice experimental trick for alignment, which takes advantage of the cross-talk between the detectors with one of the dyes. The solution of the dye is illuminated with one of the lasers and the autocorrelation functions of both detectors' outputs is measured. As both of the detectors see the same concentration of the dye, the two autocorrelation functions should be identical if the sampling volumes for both detectors are equal. Next, one can check the overlap of the two volumes by cross-correlating the outputs of the detectors: if the cross-correlation function is equal to both of the autocorrelation functions, the overlap is achieved. The alignment procedure thus appears to be elegant but rather cumbersome. Furthermore Schwille *et al* (1997) point out that the measurement is very sensitive to the quality of the objective. For example, proper alignment was achieved with a Zeiss Plan Neofluar 40×0.9 objective but failed with a Zeiss Plan Neofluar 63×1.2 water immersion objective. Yet with the right choice of dyes and careful alignment the authors could resolve bound fractions as low as 1%.

As pointed out in the instrumentation section, this alignment problem is resolved by the use of a single laser to excite both species: multiple lines of the same laser (Winkler *et al* 1999) or by two-photon excitation (Heinze *et al* 2000).

In conclusion, the implementation of FCS to measure binding interaction of biomolecules is as diverse as the experimental systems under study. For each assay, one must optimize the fluorescence labelling and the FCS setup (one colour versus two colour) to maximize the binding signature in the correlation curve. The dynamic range for these measurements can reach up to three decades in the concentration of complexes.

4.5. Conformational fluctuations of biomolecules

In this section, we discuss the application of FCS to monitor the dynamics of conformational fluctuations of biomolecules. Two systems have been studied extensively in the last five years: the GFP and DNA molecules.

In the case of GFP, the protein's fluorescence emission has been known to be subject to dynamic fluctuations since 1997 (Dickson *et al* 1997). These fluctuations are associated with structural changes within a protein and are sensitive to the molecular environment (in particular to the concentration of protons i.e. the pH). Thus, the research (Haupts *et al* 1998, Widengren *et al* 1999a, 1999b, Schwille *et al* 2000) on GFP fluctuations in fluorescence addresses two main issues: (1) the nature of the structural changes leading to the fluctuations in fluorescence emission, and (2) the possibility of probing local pH through the FCS measurement of GFP fluctuations (the special interest is ultimately in probing the intracellular environment).

In the case of DNA molecules, FCS has been implemented to monitor the dynamics of conformational thermal fluctuations and to better understand the kinetics and the thermodynamics of secondary structure formation.

4.5.1. Protonation of GFP. As presented in section 4.1, the GFP is a naturally fluorescent protein. The chromophore of GFP is formed spontaneously by three residues embedded within a barrel of β-sheet domains. The photodynamical characteristics of this chromophore are greatly influenced by the concentration of protons in its surroundings. In the case of the widely used modification of GFP, EGFP (GFP-F64L/S65T), the normalized absorption at 488 nm, fluorescence excitation at 490 nm and emission at 510 nm all follow a pH dependence, consistent with a simple molecular mechanism: binding of a proton (protonation) to EGFPs chromophore prevents its excitation and thus its fluorescence (Haupts *et al* 1998).

Furthermore, Haupts *et al* (1998) point out that the EGFPs chromophore can be protonated not only by binding an external H^+ ion from solution, but also through the transfer of a proton from an internal hydroxyl group (figure 5). Haupts *et al* (1998) perform FCS measurements on EGFP at different pH and fit the autocorrelation functions with the expression which is similar to (23) but has two chemical kinetics terms instead of just one in order to account for two protonation pathways:

$$G(t) = \frac{1}{\bar{N}}\left(1+\frac{t}{\tau_D}\right)^{-1}\left(1+\frac{t}{\omega^2\tau_D}\right)^{-1/2}\left(1+P\,\mathrm{e}^{-t/\tau_C}+P'\,\mathrm{e}^{-t/\tau_C'}\right)$$

where τ_D is the diffusion time scale, ω is the aspect ratio of the confocal volume, τ_C and τ_C' are the external and the internal protonation time scales, respectively, and P and P' are related to equilibrium constants.

The mutant GFP-Y66W, whose chromophore does not contain any internal hydroxyl group prone to protonation, can be used as a control, to determine some of the parameters

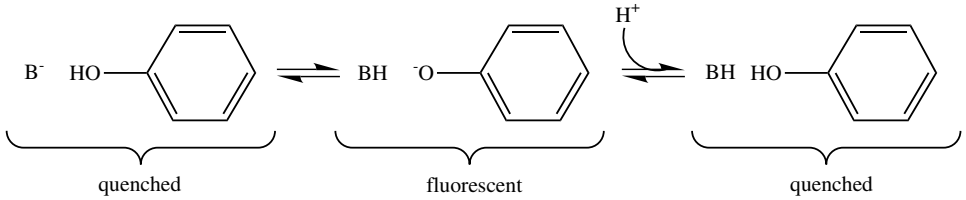

Figure 5. The two pathways of protonation of GFP chromophore (from Haupts *et al* (1998), copyright 1998 National Academy of Sciences, USA). Only A^-, the non-protonated state, is fluorescent, while both protonated states, AH and AH', do not emit light.

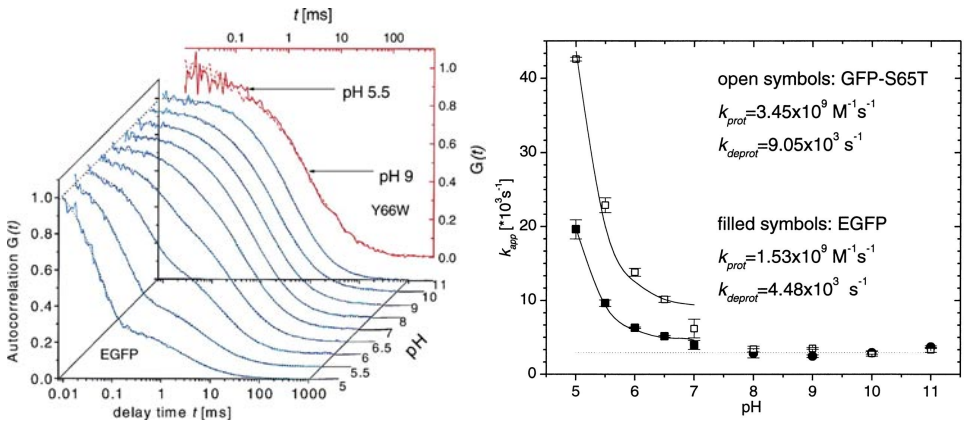

Figure 6. (*A*) FCS cross-correlation curves for the fluorescence fluctuations of EGFP at different pH (from Haupts *et al* (1998), copyright 1998 National Academy of Sciences, USA). As pH decreases, a fast conformational transition is unravelled, and analysed as an exchange of proton with the buffer. Note that, at high pH, the FCS correlation function from EGFP can be fitted with one diffusion contribution and one slow chemical fluctuation step, associated with an internal protonation. (*B*) The analysis of the fluorescence fluctuations yields the pH dependence of the apparent external protonation rate $k_{\mathrm{app}} = k_{\mathrm{protonation}}[\mathrm{H}^+] + k_{\mathrm{deprotonation}}$, whose pH dependence is fitted to give $k_{\mathrm{protonation}}$ and $k_{\mathrm{deprotonation}}$.

independently (figure 6). Thus, a robust measurement of τ_C can be achieved. The dependence of this time scale on the pH yields the rates of interaction with protons in the bulk solution:

$$\frac{1}{\tau_C} \approx k_{\mathrm{protonation}}[\mathrm{H}^+] + k_{\mathrm{deprotonation}} \Rightarrow \begin{cases} k_{\mathrm{protonation}} = (1.53 \pm 0.06) \times 10^9\ \mathrm{M}^{-1}\ \mathrm{s}^{-1}, \\ k_{\mathrm{deprotonation}} = (4.48 \pm 0.27) \times 10^3\ \mathrm{s}^{-1}. \end{cases}$$

These measurements confirm nicely the bulk measurement of the protonation equilibrium:

$$pK_A = \log\left(\frac{k_{\mathrm{protonation}}}{k_{\mathrm{deprotonation}}}\right) = 5.5 \pm 0.3.$$

Temperature dependence of the protonation equilibrium as well as the influence of viscosity change characterize the measured fluctuations as an external protonation reaction.

Thus, the analysis of fluorescence fluctuation in GFP by Haupts *et al* (1998) identifies two protonation pathways accounting for the fluorescence fluctuations of GFP. FCS is applied here in a very controlled setting, limiting the number of parameters in the fit by using control experiments with mutant proteins, and comparing with bulk results.

The pH dependence of the fluorescence emission of EGFP is interesting for applications in living cells: the experimenter could measure the internal pH of different organelles,

by specifically targeting EGFP by fusion with a localization molecule. A simpler pH determination by analysis of EGFP fluorescence had been introduced before, relying on ratiometric measurements on EGFP emission (Kneen *et al* 1998, Llopis *et al* 1998, Miesenbock *et al* 1998). However, FCS enables the experimenter to achieve a robust (i.e. independent of GFP concentration) determination of the state of protonation.

Widengren *et al* (1999a) and Schwille *et al* (2000) documented further the fluctuations of fluorescence emission of GFP. Both unravelled fast photo-induced isomerization of the chromophore, yielding fluctuations of the fluorescence emission. GFP and its mutant are known to undergo conformational changes, switching the chromophore to a dark state upon excitation (flickering), even at basic pH. The discovery of GFP flickering (Dickson *et al* 1997) has been made at low excitation power (0.5–2.0 kW cm^{-2}), with a lifetime of the dark state above 1 s at neutral pH. Widengren *et al* and Schwille *et al* use confocal FCS to document the dependence of the flickering rate with the excitation intensity between 5 and 50 kW cm^{-2}, at pH 8.0. This range of excitation powers implies a faster flickering rate (above 1 kHz), and makes the fluorescence fluctuation of GFP detectable during its diffusion through the confocal volume. The two papers show that the GFPs flickering rate is linearly dependent with the excitation intensity, and essentially pH- and viscosity-independent. Thus flickering between bright and dark states in GFP is a light-driven transition. This result, documented by confocal FCS, is important to our understanding of the GFPs 'failures' in fluorescent emission.

4.5.2. Conformational fluctuations of DNA molecules. DNA molecules constitute a model system of biomolecular folding. Yet, most of our knowledge on the dynamics of nucleic acid folding–defolding came from bulk measurement of UV absorption or calorimetry (Cantor and Schimmel 1980, Daune 1999). The development of DNA bioconjugation chemistry enabled the experimenter to attach fluorophores and quenchers at specific locations in order to generate a spectrometric report of base proximity (see section 4.1). Consequently, enough photons can be collected from individual fluorescent objects, opening up the development of single-molecule spectroscopic techniques, and FCS in particular.

Let us present the example of the molecular beacons, a DNA probe designed by Tyagi and Kramer (1996) to detect specific oligonucleotides in solution. Molecular beacons are single strands of DNA whose sequence imposes a spontaneous folding into a hairpin loop (figure 7). A fluorophore (e.g. Rhodamine 6G) and a quencher (DABCYL) are covalently attached at the two ends of the DNA molecule, such that, when the hairpin loop is closed, fluorophore and quencher are in close proximity and the fluorescence is quenched. When the hairpin loop opens up, fluorophore and quencher are pulled apart and the fluorescence of the dye is restored. Thus molecular beacons serve as a probe of the conformational states of a DNA oligomer, as they couple a fluorescence switching with a conformational transition.

In solution, a molecular beacon spontaneously fluctuates between its closed state and its open state, and these conformational fluctuations create fluorescence fluctuations which can be monitored by FCS (Bonnet *et al* 1998, Goddard *et al* 2000). Molecular beacons are ideal probes to address the issue of the dynamics of DNA hairpin-loop conformational fluctuations for two reasons. First, their excellent fluorescence signal/background (the fluorescence of the open beacon is at least 60 times larger than the fluorescence of the closed beacon) makes the detection of the fluctuations very sensitive. Second, the conformational fluctuations follow *à priori* simple kinetics with only two states:

$$\text{Closed beacon} \underset{\tau_+}{\overset{\tau_-}{\rightleftharpoons}} \text{Open beacon}$$

where τ_- is the opening time scale and τ_+ is the closing time scale (see also figure 7).

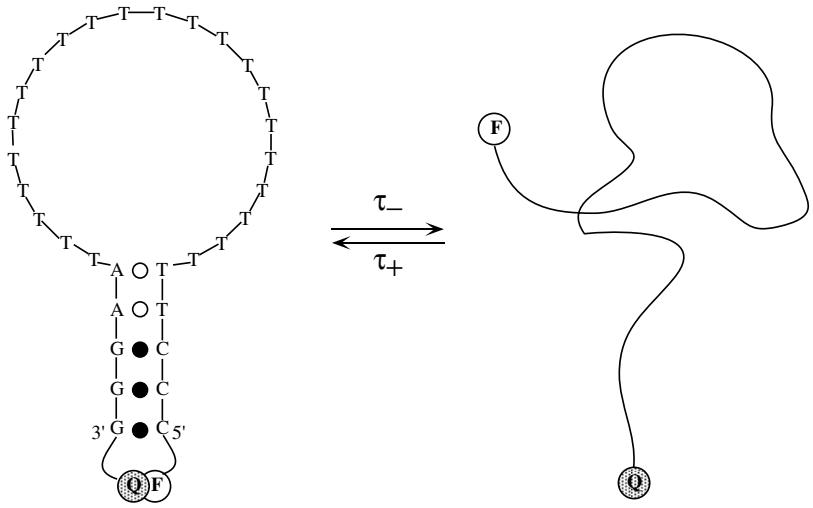

Figure 7. Schematics of the molecular beacon fluctuations. In the closed state, fluorophore (F) and quencher (Q) are in close proximity and the fluorescence is quenched. In the open state, the molecular beacon is a random coil of DNA and F and Q are pulled apart: the fluorescence is restored. The fluorescence fluctuations associated with the conformational fluctuations are analysed by FCS to prove the all-or-nothing nature of the transition, and yield information on the dynamics of the hairpin.

The autocorrelation function of the fluorescence collected from a dilute solution of molecular beacons can be described with an equation of the type (23) for isomerization reactions. The correlation function is thus a product of a diffusion term and a chemical kinetics term:

$$G_{\text{beacon}}(t) = G_{\text{diff}}(t)\, G_{\text{chem}}(t) = \frac{1}{\bar{N}}\left(1 + \frac{\tau}{\tau_D}\right)^{-1}\left(\alpha + \beta\ \exp\left(-\frac{t}{\tau}\right)\right)$$

where for simplicity a 2D approximation (19) was taken for the diffusion term; $\bar{N}$ is the average number of molecular beacons in the confocal volume, α and β are the amplitude factors related to the equilibrium constant and introduced to account for the residual fluorescence of the closed beacons and τ is the chemical relaxation time scale:

$$\tau = \left(\frac{1}{\tau_-} + \frac{1}{\tau_+}\right)^{-1}.$$

However, the direct fit with equation (23) is not reliable since the chemical relaxation time scales (between 5 μs and 1 ms, depending on the sequence of the molecular beacon) overlap with the diffusional relaxation which occupies a broad range of time scales around $\tau_D \approx 150$ μs. Then, to extract a reliable measurement of τ, Bonnet *et al* (1998) use a control molecule similar to the molecular beacons, with a fluorophore but no quencher. The fluorescence of this construct depends only weakly on its conformation and the autocorrelation function of its fluorescence fluctuations consists only of a diffusion contribution:

$$G_{\text{control}}(t) = G_{\text{diff}}(t) = \frac{1}{\bar{N}}\left(1 + \frac{t}{\tau_D}\right)^{-1}$$

such that the ratio $G(t) = G_{\text{beacon}}(t)/G_{\text{control}}(t)$ isolates the chemical relaxation kinetics (figure 8):

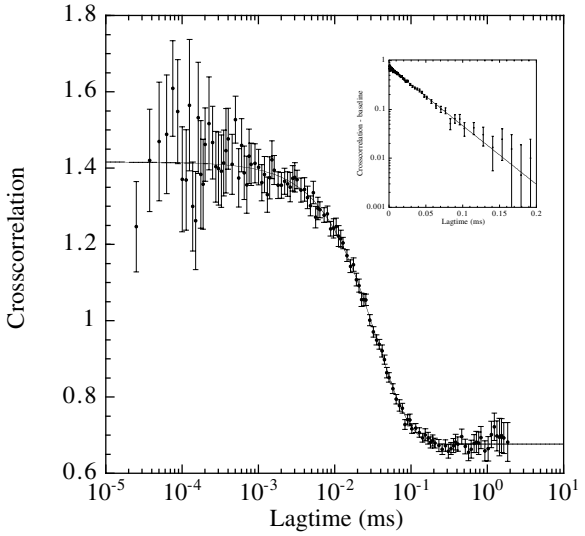

Figure 8. The contribution of DNA hairpin conformational fluctuations to the correlation function, isolated from the diffusion part by taking the ratio of FCS correlation curves for the molecular beacon and its control. The line is a mono-exponential fit yielding the characteristic time of fluctuations (inset: semi-log plot of the cross-correlation function emphasizes the validity of the mono-exponential fit). In this experiment, the molecular beacon has a 5-base stem and a 21-thymidine loop. These fluctuations are measured at 45 °C in 0.1 M NaCl and 10 mM TrisCl, pH 8.0.

$$G(t) = \alpha + \beta \exp\left(-\frac{t}{\tau}\right).$$

The quality of the fit validates the two-state model presented for the thermal fluctuations of the molecular beacon and allows one to measure the chemical relaxation time τ.

An additional measurement is used to obtain opening and closing time scales of the molecular beacon separately. The fluorescence melting curve of the molecular beacon (measured in bulk solution in a fluorometer) yields the equilibrium constant of the transition as a function of temperature:

$$K(T) = \frac{\tau_+}{\tau_-}$$

such that one can extract a reliable measure of τ_- and τ_+:

$$\tau_- = \tau \ \frac{1+K}{K}$$
$$\tau_+ = \tau \ (1+K).$$

Measurements of τ and K are made at different temperatures (between 10 and 50 °C) to yield an Arrhenius plot of the opening and closing time scales. Thus the activation enthalpies associated with the two transitions are determined.

This procedure has been applied to the molecular beacons of different loop sequences and loop lengths. The closing time is shown to increase with the length of the loop. However, the estimation for the scaling exponent of 2.6 for the thymidine loops, measured by Bonnet *et al* (1998), is higher than the 1.8 predicted by the classical excluded-volume polymer chain model. The discrepancy indicates that the stiffness of short chains (the loop lengths were in the

range from 12 to 30 nucleotides) of single-stranded DNA is larger than anticipated, probably due to the strong excluded-volume interaction.

The base composition of the loop has also been shown to influence drastically the closing kinetics of the molecular beacon. Adenosine loops, unlike thymidine loops, present a significant energy barrier for closing. Consequently the characteristic time scale can also be very different: a loop, composed of 21 adenosines, is 20 times slower to close than a loop composed of 21 thymidines, at 10 °C in 0.1 M NaCl buffer (Bonnet *et al* 1998). Goddard *et al* (2000) studied systematically the kinetics of closing of molecular beacons and showed that the activation energy associated with its closing increases linearly with the length of the loop for poly-adenosines (for loops from 8 to 30 bases long), and is essentially constant for poly-thymidines. This is interpreted with the known base stacking of single-stranded poly-adenosines: when a beacon is open, its loop adopts a rigid stacked structure such that destacking of the single strand is a limiting step towards closure of the hairpin loop structure.

Other FCS studies of DNA conformational fluctuations have been reported. Edman *et al* (1996) studied the fluctuations of TMR emission in the vicinity of DNA. The dye is covalently attached to an 18-base oligonucleotide which is then specifically hybridized to a large single-stranded DNA. First, the measurement of the pulsed-excitation fluorescence decay of TMR is performed and two characteristic fluorescence lifetimes found. Edman *et al* (1996) argue that the intercalation of TMR with the neighbouring DNA bases could explain the shorter lifetime of the dye. Then, a characterization of the kinetics of TMR fluctuations is attempted using FCS. Edman *et al* (1996) propose to fit the autocorrelation function of fluorescence fluctuations with a diffusive relaxation convoluted with a stretched exponential relaxation to account for the heterogeneity of relaxation kinetics:

$$G(t) = \frac{1}{\bar{N}} \left(1 + \frac{t}{\tau_D}\right)^{-1} \left(1 + \frac{t}{\omega^2 \tau_D}\right)^{-1/2} \left(1 + A \ \exp\left(-(kt)^{\beta}\right)\right).$$

This five-parameter fit yields a characteristic time scale of 23 ms and a stretched exponent of 0.44 for the chemical fluctuations.

Wennmalm *et al* (1997) get rid of the diffusion contribution to reduce the number of parameters in the fit: they grafted their DNA construct with a TMR at one end, and a biotin at the other, onto a streptavin-coated coverslip. In this case, the photobleaching of the dye limits the accumulation time (in this realization of confocal FCS, the lifetime of the dye is about 1 s). Thus in order to accumulate statistics, Wennmalm *et al* (1997) scan the sample for DNA molecules measuring the correlation function at each spot for 1 s (while checking that the dye did not bleach during the measurement), and then average all of the measurements. The measured autocorrelation functions are also fitted with a stretched exponential with $\beta \approx 0.44$ and $k^{-1} = 250$ ms. The discrepancy of time scales with the paper of Edman *et al* (1996), as well as the absence of a microscopic mechanism justifying the stretched exponential, make the interpretation of the results of these two papers difficult.

4.6. FCS in living cells

In this section, we present the application of FCS in living cells, made possible by the development of confocal FCS. In particular we discuss the determination of absolute concentrations of proteins and measuring proteins' or nucleic acids' mobility in living cells.

4.6.1. Counting fluorescent particles in vivo. To understand living cells' phenotype, it is often necessary to extrapolate *in vitro* results on enzymatic (protein-catalyzed) reactions to *in vivo* situations. This requires prior knowledge of the absolute concentration of biomolecules

of interest within the cells. Fluorescence tagging of these biomolecules could allow their quantification, but this measurement is only relative and hard to calibrate. Indeed, the fluorescence of individual tags can be affected by the local pH environment or the presence of electron-acceptor quenchers (such as oxygen or aromatic groups). FCS provides an elegant non-invasive tool to measure the absolute concentration of a fluorescently tagged protein *in vivo*.

As shown in the theoretical section, the amplitude of a FCS autocorrelation function is inversely proportional to the average number of fluorescent particles within the sampling volume:

$$G(0) = \frac{1}{\bar{N}}.$$

Thus, once the confocal volume of the FCS setup is calibrated, the absolute concentration of fluorescent particles can be obtained. Note that this determination of the concentration is accurate if all fluorescent proteins are mobile within the confocal volume.

Cluzel *et al* (2000) used FCS to count fluorescent proteins in living cells. The biological question addressed was the dependence of the tumbling rate of the *E. coli* flagellum on the concentration of the protein which regulates it, the phosphorylated kinase CheY-P. A fusion construct of CheY-P with GFP (cf section 4.1) was prepared and cloned in *E. coli*, while a latex bead was attached to the bacteria's flagellum to monitor its rotation. The analysis coupled a video-monitoring of the rotation of the bead (to determine the tumbling rate of the flagellum) with an FCS measurement on the CheY-P/GFP (to determine their absolute number within the confocal volume). In a calibration measurement, Cluzel *et al* (2000) found a linear relationship between the measured concentration of CheY-P/GFP and the collected fluorescence. This proves that the immobile fraction of proteins is negligible and the FCS calibration accurate: there are few binding sites for the fusion protein in the bacterium.

The resulting titration curve is a first example of an enzymology measurement at the single-cell level: the input/ouput relationship can be fitted by a Hill function with an equilibrium constant of 3.1 μmol and a Hill coefficient of 10.3 ± 1.1. The steepness of the curve (hinting towards a tightly regulated amplification mechanism in the signal transduction of chemotaxis) had been obscured in previous studies, which measured the properties averaged over the ensemble of living cells. It was unravelled due to the possibility of performing cell-by-cell fluorescence analysis with FCS. In this study, FCS is used mostly as a calibrating technique of fluorescence, to study quantitatively biochemical and genetic pathways within living cells.

4.6.2. Probing living cells' organelles with FCS. The release of the commercial confocal FCS setup by Zeiss offers a new tool to cell biologists eager to probe living cells. One advantage of FCS is the amplification of the detection signal/noise of fluorescent particles. Indeed, for microscopists, living cells generate a very high autofluorescence, making single fluorophore detection still challenging (except in the particular case of membrane-bound fluorophores). The autocorrelation function in FCS is a tool for signal processing which amplifies the correlated signal from brightly fluorescent particles above the background signal.

Brock *et al* (1998) have presented the application of FCS to characterize the GFPs fusion proteins *in vivo* (cf section 4.5.1). The protein of interest is the epidermal growth factor receptor (EGFR) which can be found on the PM, in the cytoplasm, or in the endoplasmic reticulum (ER). The spatial distribution of EGFR between these three cellular loci results from a dynamic equilibrium of the exchange between compartments. Brock *et al* (1998) use FCS to rapidly characterize the distribution of a fusion construct EGFR/GFP. The alternate prospect of this work is the development of a drug-screening protocol, whereby drugs against EGFR

would be tested for their ability to disrupt the EGFR spatial distribution. Confocal FCS is here crucial to identify the loci of interest (PM, cytoplasm, ER) before analysing the EGFR/GFP dynamics.

Brock *et al* (1998) measure a complex autocorrelation function for the diffusion of EGFR/GFP. They invoke a nine-parameter diffusion model to accurately fit the FCS curve:

$$G(t) = \frac{1}{\bar{N}}\left(1 + \frac{p}{1-p}\exp\left(-\frac{t}{\tau_{\text{triplet}}}\right)\right)\sum_{i=1}^{3}\frac{\phi_i}{\left(1+\frac{t}{\tau_{Di}}\right)\sqrt{1+\frac{t}{\omega^2\tau_{Di}}}}$$

where ϕ_I is the fraction and τ_{Di} is the transversal diffusion constant for the species i, and τ_{triplet} and p are the lifetime and the fraction of GFP in the triplet state. In all cell compartments, a fast diffusion process is observed ($D \approx 1.9 \times 10^{-7}$ cm^2 s^{-1}), more prominent in the cytoplasm and the ER (up to 80% of the molecules) than in PM (only 35%): this diffusion is characteristic of free EGFR/GFP in solution. A slower kinetics (with D around 3×10^{-9} cm^2 s^{-1}) is also present as a signature of EGFP/GFP interacting with the cellular environment. These results are shown to be consistent with FRAP measurements in the same system, but Brock *et al* (1998) point out that FCS measurements require lower concentrations of GFP, are faster to acquire and less disruptive for the cells.

The analysis of the fast component of diffusion has been refined by Gennerich and Schild (2000). First, they report on a surprising observation: the FCS measurement of the diffusion of short TMR-labelled dextran polymers (10 kDa) in the dendrites of cultured neurons yields a diffusion constant larger than the same measurement in water solution. This result is surprising since the interior of a cell is *a priori* more viscous than water. The paradox stems from the fact that the standard FCS diffusion equation (18) cannot be applied to molecules whose motion is restricted in some of the directions to the dimensions comparable or smaller than those of the confocal detection volume. Thus, Generich and Schild introduce a refinement of the FCS model to include the confinement of the detection volume. The thermal motion in small cellular compartments is modelled essentially as a corrected mono-dimensional diffusion. An approximated fit is proposed for a diffusion confined in two directions (i.e. diffusion in a tunnel-like geometry similar to that of a neuronal dendrite):

$$G(t) = \frac{1}{\pi w_{xy}^2 d_z C}\sqrt{\frac{1}{1+\frac{t}{\tau_D}}}\, g_{Y,\tau_D}(t)$$

with

$$g_{Y,\tau_D}(t) = \frac{\sqrt{\pi}}{Y}\left[1 + \left(\frac{Y}{\sqrt{\pi}}\frac{\operatorname{erf}(Y)}{\operatorname{erf}^2(Y/\sqrt{2})} - 1\right)\frac{\exp\left[-k(Y)(\pi/Y)^2\frac{t}{\tau_D}\right]}{\sqrt{1+\frac{t}{\tau_D}}}\right]$$

$$k(Y) = 0.689 + 0.34\,\mathrm{e}^{-0.37(Y-0.5)^2} \qquad \text{and} \qquad \tau_D = \frac{w_{xy}^2}{4D}$$

where w_{xy} is the excitation beam waist, d_z and d_y are the longitudinal and transversal dimensions of the confinement volume, C is the concentration of fluorescent molecules, D is the diffusion constant and Y is the confinement parameter ($Y = d_y/r_{xy}$).

The bonus of this restricted-diffusion model is that the size of the confinement volume can be estimated from the fit. For example, in the case of the dendrites of cultured neurons, Generich and Schild measure a transversal dimension of 0.65 μm, very consistent with a line scanning profile of the dendrites. This refinement of the diffusion fit shows how the analytical treatment of a FCS measurement can yield sub-microscopic information on a system.

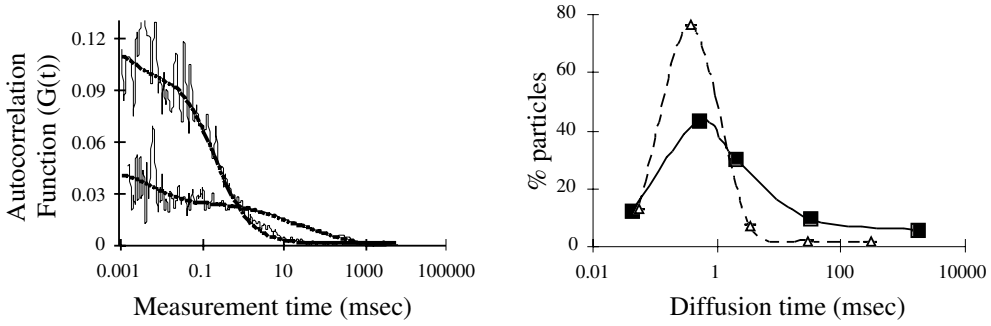

Figure 9. Measurement of the intranuclear diffusion and interaction state of DNA probes in living cells by FCS (from Politz *et al* (1998), copyright 1998 National Academy of Sciences, USA). Left panel: FCS measurements and corresponding fit for the diffusion of fluorescently labelled oligo (dT) (low-amplitude curve) and oligo (dA) (large-amplitude curve) inside cell nuclei. Right panel: corresponding distributions of particles for the five diffusion rates used in the fit of the FCS autocorrelation functions from the left panel. This measurement monitors the slower diffusion of the oligo (dT) probes compared to the oligo (dA) probes because of the hybridization of the oligo (dT) to nuclear mRNA poly (A) tails.

4.6.3. Probing living cells' nuclear structure with FCS. Politz *et al* (1998) carried out FCS measurements in living cells to probe intranuclear diffusion and concentration of messenger RNA in their nucleus. Understanding the structure of the cell nucleus and the dynamics of gene expression within it is one of the major challenges of cell biology. Messenger RNA (mRNA) synthesis and its shuttling out of the nucleus are studied here with fluorescently labelled poly-oligonucleotides. At the end of transcription the cellular genetic machinery appends to all mRNA a universal oligo-ribo-adenosine (poly-A) tail. This tail is accessible for hybridization by a complementary oligo-deoxyribo-thymidine (poly-dT). As a result of this hybridization the mobility of the poly-dT decreases. Thus, Politz *et al* (1998) use a fluorescently labelled poly-dT and the FCS technique to probe the presence of mRNAs' poly-A in living cells. Poly-dA, as well as prehybridized poly-dT, are used for control experiments as non-hybridizing probes to mRNA.

The experimental setup for this study is the commercial Zeiss and Evotec's confocor system. The FCS curves are fitted with a ten-parameter model, superposing the diffusion of five species (see section 2.3):

$$G(t) = \sum_{i=1}^{5} \frac{A_i}{\left(1 + \frac{t}{\tau_{Di}}\right)\sqrt{1 + \omega^2 \frac{t}{\tau_{Di}}}}.$$

In all measurements, a fast diffusing species with a characteristic time scale (40 μs) contributes 12% of the sum. Surprisingly, this is faster than the diffusion time scale of the same molecules in solution, and the 'channelled' diffusion justification can be invoked, as in the previous section. Probes non-interacting with mRNA diffuse mostly (a fraction of about 80%) with time scales in the 100 μs–1 ms domain, whereas poly-dT (interacting with mRNA) diffuse globally slower, with only 40% molecules in the 100 μs–1ms domain, and 40% spread above 1 ms (figure 9). The spread-out distribution of the diffusion time scales reflects the distribution of molecular sizes associated with the mRNA.

This study, presenting the first attempts at characterizing molecular diffusion *in vivo*, constitutes a benchmark for further FCS measurements in living cells. The authors present a ten-parameter fit yielding surprisingly slow (above 10 ms) and fast (around 40 μs) diffusion components. However, the authors prove that mid-range diffusion contributions

are consistently different for poly-dT and poly-dA probes (figure 9): the lower mobility of poly-dT probes compared to poly-dA, and prehybridized poly-dT is a signature of the presence and accessibility for hybridization of mRNA in the cell nucleus. The variability of the FCS results taken at different locations of the nucleus is also noteworthy. The heterogeneous density of the nuclear environment has been previously demonstrated by electron microscopy, and the localization of genes within the chromatin seems to be crucial to their accessibility to transcription factors as well as transcription machinery. Probing the heterogeneity of the cells' nuclei by FCS might shed light on a major mode of regulation of gene expression.

A systematic mapping by FCS of the mobility of EGFP in cell nuclei gives indeed a more dynamic picture of the heterogeneous structure in living cells' nuclei. Wachsmuth *et al* (2000) develop an anomalous diffusion model in confocal FCS to probe GFPs diffusion *in vivo*. FRAP measurements as well as single-molecule tracking have shown that the diffusion of biomolecules in living cells can be modelled as an obstructed diffusion. Phenomenologically, the mean square displacements of diffusing particles are

$$\langle r^2(t)\rangle = 6D_S\, t^{2/d_w}$$

where $d_w(>2)$ is related to the fractal dimension of the volume of diffusion. The resulting model for the autocorrelation function of the fluorescence of an anomalously diffusing particle is

$$G(t) = \frac{1}{\bar{N}} \frac{1}{1+\left(\frac{t}{\tau_D}\right)^{2/d_w}} \sqrt{\frac{1}{1+\omega^2\left(\frac{t}{\tau_D}\right)^{2/d_w}}}.$$

This fit, less physically plausible than Gennerich and Schild but more straightforward, is used to probe the diffusion of GFP in living cells. A map of the obstruction parameter shows that d_w averages at 2.3 in the cell nucleus, while it is essentially 2.0 (free diffusion) in the cell's cytoplasm. This anomalous diffusion of proteins in the cell's nucleus is consistent with the higher density of obstacles and binding sites within the chromatin.

In conclusion, the application of FCS to probe living cells is promising. The availability of a commercial FCS confocal microscope will most certainly multiply the number of users, and we should see more dynamic information on living cells gleaned with FCS in the coming years.

5. Techniques related to FCS

5.1. Photon counting histogram: an alternative signal analysis of single-object fluorescence

Having in mind that the progress in the photon counting techniques made possible the detection of individual fluorescent molecules, one must acknowledge that autocorrelation or cross-correlation analysis of the collected signal (as done in FCS) is only one of many possible signal processing tools.

FCS is adequate when the different fluorescence-emitting particles have a specific signature in the time domain. For example, in the case of the use of FCS in a binding assay, a small fluorescently tagged probe interacts with a large substrate and changes its diffusion coefficient. In that case, the diffusion time scales (before and after binding) are easily separated on a FCS curve, and one can measure the contribution of each in the correlation function.

However, there are some situations where the biological processes generate changes not in the time domain, but rather in the amplitude domain. Let us present one such example to illustrate the need for alternative signal processing in single-molecule fluorescence analysis.

The dimerization of receptor molecules is a crucial and ubiquitous event, solving a very general question in cell biology: how does a cell, as a closed compartment, manage to probe its surroundings (be it molecules in the medium, or neighbouring cells)? Receptors are loaded onto the cell's PM, and constantly interact with molecules (ligands). Any relevant interaction must then be transduced towards the interior of the cell, to generate a cellular response (activation of genes, exocytosis of pre-synthesized molecules, etc). One could imagine that the cells transduce the extracellular ligand-specific interaction with an intracellular change of conformation. In fact, cells use a simpler-to-design and more robust mechanism to transduce the extracellular events into intracellular ones: the dimerization of its receptors. Upon binding to a ligand, many receptors become susceptible to dimerization with another ligand-interacting receptor, bringing into close proximity their intramolecular domains previously separated. This modulation of receptor separation is then 'read' by signal transduction machinery within the cells.

What would be the microscopy technique of choice to detect such dimerization? In most cases, the density of receptors on the cell forbids any temporal–spatial resolution of individual receptors. For example there are 30 000 T-cell receptors per T cell, 10 μm in diameter, i.e. one receptor every 50 nm, or 4 per diffraction-limited spot. Standard confocal microscopy or even deconvolution microscopy will not detect individual dimerization events. One could then invoke FCS, but the resolution of monomers and dimers is impossible, as the difference of the expected diffusion coefficients is negligible.

FCS, by computing a normalized autocorrelation function, discards the information distinguishing monomers and dimers, i.e. the intrinsic fluorescence Q per object (number of photons collected per object per unit time, also called specific brightness). Specific signal processing must be carried out to measure Q.

Concomitant to the FCS revival, Qian and Elson (1990a, 1990b) proposed a statistical treatment of a fluorescence signal to distinguish fluorescent objects by their inner brightness, rather than by their mobility characteristics. This constitutes a switch from the analysis in the time domain for FCS to an analysis in the amplitude domain. The moments of the distribution of the collected fluorescence n or its deviation from the mean $\Delta n = n - \langle n \rangle$ are

$$\langle n \rangle = \sum_k Q_k \langle N_k \rangle$$

$$\langle (\Delta n)^2 \rangle = \sum_k Q_k^2 \langle N_k \rangle$$

$$\langle (\Delta n)^3 \rangle = \frac{\chi_1 \chi_3}{\chi_2^2} \sum_k Q_k^3 \langle N_k \rangle$$

where Q_k is a specific brightness of component k and $\chi_l = \int I^l(\vec{r})\,\mathrm{d}\vec{r}$ is determined by the geometry of fluorescence excitation and collection (for a purely Gaussian beam, $\chi_1\chi_3/\chi_2^2 = 4/3$). These moments are computed for essentially non-diffusing particles, i.e. the binning time of the photon collection must be shorter than the diffusion time scales (frozen limit). In the first presentation of this moment analysis, Qian and Elson used large fluorescent beads (115 and 50 nm in radius), whose characteristic translational diffusion time scale is around 200 ms while the binning time is kept at 10 ms (Qian and Elson 1990a). This moment analysis is applied successfully to the determination of the composition of a binary mixture of the two beads.

One nice aspect of an analysis with high order moments of fluorescence fluctuations is the determination of the immobile fraction among fluorescent particles. In many biological applications, a non-negligible fraction of the fluorescent probes are non-diffusing, because of binding interactions with other biomolecules, or retention in specific cellular domains.

FRAP is classically used to measure this immobile fraction, yielding a partial recovery of the fluorescence signal after photobleaching. FCS, on the other hand, does not detect the presence of an immobile fraction, as the autocorrelation function picks up the contribution of diffusing particles only (unless a special technique, like scanning FCS, is applied, see section 3.3.1). Thus, Qian and Elson proposed to use the higher order moments of the collected fluorescence n to quantify the number of mobile (N_m) and immobile (N_i) fluorophores in the sampling volume (Qian and Elson 1990b):

$$\langle n\rangle = Q\,(\langle N_i\rangle + \langle N_m\rangle)$$
$$\langle(\Delta n)^2\rangle = Q^2\langle N_m\rangle$$
$$\langle(\Delta n)^3\rangle = \frac{\chi_1\chi_3}{\chi_2^2}Q^3\langle N_m\rangle.$$

A more complete analysis of the collected fluorescence must take into account the convolution of the diffusion of the particles, in and out of the sampling volume, with the emission of the fluorescence. Both processes are intrinsically stochastic and hard to analyse analytically. The initial formalism, presented by Qian and Elson, computed the deviation of the statistics of the collected fluorescence from a simple Poissonian. This approach has been generalized by Gratton's group with the method of moment analysis, or MAFID (Chen *et al* 1999, Müller *et al* 2000). An experimentally more tractable method than MAFID has been introduced by the Evotec group, with the fluorescence-intensity distribution analysis, or FIDA (Kask *et al* 1999, 2000).

The experimental setup for MAFID or FIDA is the same as for FCS: a confocal setup with a high efficiency collection of emitted fluorescence. Only the signal processing is different: the collected photons are counted per bin of $\Delta t = 40\ \mu$s typically, instead of time-correlated. If the fluorescent particles were immobile and emitting with a total inner brightness Q, one would get a pure Poissonian statistics for the number n of photons per bin:

$$P(n) = \frac{(Q\,\Delta t)^n}{n!}\mathrm{e}^{-Q\,\Delta t}.$$

In the real situation, the number of fluorescent particles, within the sampling volume, is fluctuating. Thus to compute the number of collected photons per bin, one must use conditional probabilities (Kask *et al* 1999):

$$P(n, \mathrm{d}V_i) = \sum_{m=1}^{\infty} P(n|m, \mathrm{d}V_i)q(m)$$

where $q(m)$ is the probability of having m fluorescent particles within the sampling volume $\mathrm{d}V_i$ and $P(n|m, \mathrm{d}V_i)$ is the probability of collecting n photons, given that m fluorescent objects were in the volume $\mathrm{d}V_i$. Both distributions are then Poissonian, fully characterized by the concentration of fluorescent particles C, their inner brightness Q and the excitation/collection profile $I\,(\vec{r}) = I_0 B\,(\vec{r})$ ($B\,(\vec{r})$ is the excitation/collection profile normalized to 1 at maximum).

The technical trick consists in computing the generating function:

$$g(\xi) = \sum_{n=0}^{\infty} P(n)\xi^n = \sum_{n=0}^{\infty}\sum_i P(n, \mathrm{d}V_i)\xi^n$$
$$= \sum_i \exp\left[C\,\mathrm{d}V_i\left(\mathrm{e}^{(\xi-1)QB(\vec{r})} - 1\right)\right] \approx \exp\left[\int_V \mathrm{d}V\,C\left(\mathrm{e}^{(\xi-1)QB(\vec{r})} - 1\right)\right].$$

Kask *et al* (1999) pointed out how the use of the generating function is crucial to fit the histograms generated by FIDA: the logarithm of the generating function for multiple non-interacting species is simply the sum of the logarithm of the individual generating functions (a consequence of the statistical independence of the fluorescence emission).

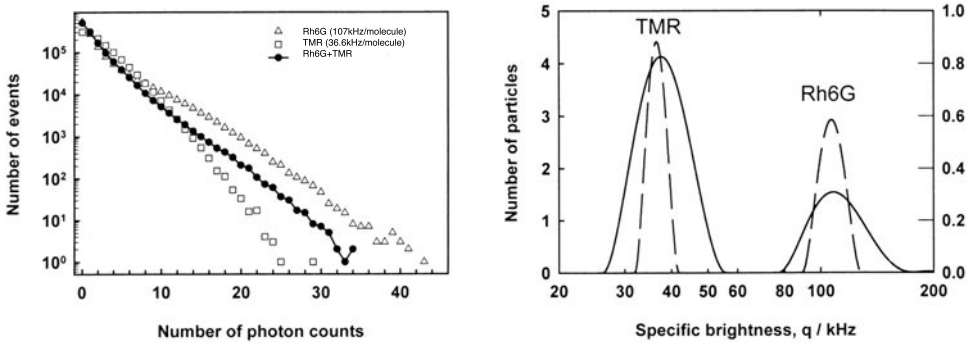

Figure 10. Fluorescence intensity distribution analysis for solutions of pure dyes (from Kask *et al* (1999), copyright 1999 National Academy of Sciences, USA). Left panel: Distribution of collected photons for a solution 0.5 nmol Rh6G, or 1.5 nM TMR, or a mixture of the two dyes (0.8 nMTMR + 0.1 nM Rh6G) is measured for a binning time of 40 μs. Right panel: Distribution of particles of different brightness as derived by the FIDA fit. This FIDA analysis resolves the heterogeneity of fluorescence in this mixture of Rh6G and TMR, while an FCS analysis would not have resolved these two dyes because of their comparable diffusion coefficients.

When taking $\xi = \mathrm{e}^{\mathrm{i}\varphi}$, the generating function is the Fourier transform of the distribution $P(n)$.

For a solution of many species $j = 1, 2, \ldots$ (with an inner brightness Q_j and a concentration C_j), the generating function is

$$g(\xi) = \exp\left[\sum_j C_j \int_V \left(\mathrm{e}^{(\xi-1)Q_j B(\vec{r})} - 1\right)\right].$$

Contrary to FCS, there is no analytical expression for the fitting curve, because of the intractable integration over the spatial excitation profile. Kask *et al* (1999) show that a careful numerical integration is sufficient to the resolution of FIDA. However, the classical Gaussian excitation profile is not accurate and the authors use an overstretched Lorentzian profile to carry out the numerical integration. This profile can be calibrated with a single-species experiment, such as the number of variables in the fit of a FIDA experiment is limited to twice the number of species (one concentration and one inner brightness per species).

The fit of the distribution $P(n)$ is then $P(n) = FFT^{-1}(g(\mathrm{e}^{\mathrm{i}\varphi}))$. As shown in figure 10, a mixture of two fluorescent dyes of different brightnesses can be resolved by FIDA: one can measure the specific brightness as well as the concentration of each species.

The FIDA analysis has been extended for a two-detector case (Kask *et al* 2000). The analysis follows naturally from the 1D case. The two detectors can be assigned to two different polarizations of the emitted light (a particularly useful scheme if the heterogeneity of the sample yields a distribution of rotational diffusion coefficient) or to two different colours.

The success of the FIDA method is evident from its booming application in the drug-screening industry.

The collection of fluorescence per static bin allows the establishment of the analytical expression for the distribution of collected photons. The choice of the binning time Δt is arbitrary, although constrained by the need to approximate the fluorescent particles as immobile: Δt is taken to be 40 μs, smaller than the typical dwell time of a fluorescent object in the field of view (>200 μs). This approximation discards all the information that the FCS analysis was providing on the dynamics of the fluorescent objects. Is there a way to reconcile the two approaches and gain information on the particle dynamics at the same time as on their inner fluorescence?

Very recently, Palo *et al* (2000) proposed a method derived from FIDA to resolve the diffusion times and molecular brightness in a single experiment. The idea is to systematically record the histogram of the collected fluorescence for different binning times Δt (from 40 μs to 2 ms). These histograms are analysed by FIDA to yield apparent concentration $C_{\rm app}$ and apparent molecular brightness $Q_{\rm app}$ for each value of Δt:

$$C_{\rm app}(\Delta t)Q_{\rm app}(\Delta t) \times \Delta t = \langle n \rangle$$
$$C_{\rm app}(\Delta t)Q^2_{\rm app}(\Delta t) \times (\Delta t)^2 = \langle n(n-1) \rangle - \langle n \rangle^2.$$

Using the autocorrelation function of FCS, $G(t)$, and introducing

$$\Gamma(\Delta t) = \frac{1}{CQ^2\Delta t}\int_0^{\Delta t} {\rm d}t_1 \int_0^{\Delta t} {\rm d}t_2\, G(t_2 - t_1)$$

Palo *et al* (2000) get

$$C_{\rm app}(\Delta t) = \frac{C_{\rm app}(0)}{\Gamma(\Delta t)} = \frac{C}{\Gamma(\Delta t)} \qquad \text{and} \qquad Q_{\rm app}(\Delta t) = Q_{\rm app}(0)\Gamma(\Delta t) = Q\Gamma(\Delta t).$$

FIDA analysis is thus carried out for each binning time Δt, yielding $C_{\rm app}(\Delta t)$ and $Q_{\rm app}(\Delta t)$. Tuning the diffusion coefficient D in $G(t)$ to match $\Gamma(t)$ to these apparent parameters allows a complete determination of the absolute concentration C, molecular brightness Q and D. Palo *et al* (2000) present one simulation where three molecular species are resolved with no prior calibration. This *tour-de-force* of statistical analysis will certainly be used to resolve the heterogeneity in molecular brightness or in the diffusion constant of a sample.

In fact, recent developments in electronic counters and the accessibility of large computer RAM allow the experimenter to collect all the information on the photons emitted and collected from the sampling volume. The collection of photons from diffusing fluorescent particles gives a series of the dwell time $\{\Delta\tau_i\}_{i=1\ldots N}$ between individual photons. Typically, for a solution of Rh6G at 1 nmol (one molecule per confocal volume), excited at 30 kW cm^{-2} (i.e. a brightness of 70 000 collected photons per second per Rh6G), one could collect the dwell times in 8-bit format during 1824 s = 30 min before using 128 Mbyte of RAM, or 128×10^6 photons. Typical counters run with a 100 MHz clock, fast enough to record all TTL pulses generated by a photodetector. All the information is in that time series, and it is up to the experimenter to decide what signal processing (FCS, MAFID, FIDA or other) is to be applied. Future studies most likely will use the analytical tools of statistical field theory to solve analytically the convolution of the diffusion and fluorescence emission statistics, and propose more and more sophisticated statistical analysis to decipher the heterogeneous composition of a sample.

5.2. Single-molecule techniques

Recently a number of techniques have emerged which allow one to detect and manipulate single biological molecules (for reviews see Xie and Trautman (1998), Mehta *et al* (1999), Schmidt *et al* (1999), Weiss (1999, 2000), Xie and Lu (1999), Clausen-Schaumann *et al* (2000), Strick *et al* (2000), Yanagida *et al* (2000)). Performing experimental measurements at a single-molecule level (a technical challenge not to be overlooked) is often necessary to address specific issues related to the complexity of biological systems. For example, the dynamics of biological macromolecules (e.g. diffusion or conformational fluctuations) often cannot be characterized with a single parameter (e.g. a diffusion constant or an energy barrier), as for small molecules, but rather with a distribution of these parameters. The distribution arises from small differences in sequence, conformation or local environment of the biomolecules. Furthermore, in the kinetic processes, molecules while progressing from their initial state to

the final state can pass through a number of short-lived intermediate states. Resolving these states as well as the distribution of dynamic parameters is often not achievable in an ensemble averaging measurement: it would involve a synchronization of the dynamics of all of the molecules, which is neither easy nor always possible, as well as requiring a sensitivity to the distributed dynamics.

We are not attempting to present here a thorough review of the single-molecule methodology. Instead, we will focus on two of the single-molecule imaging applications which share with FCS the idea of performing statistical analysis of the fluorescence signal in order to extract information on chemical kinetics and diffusion.

5.2.1. Chemical kinetics on single molecules. The experiments by Lu *et al* (1998) addressed the questions closely related to the protein folding problem, the biological problem which proved to be extremely attractive to physical modelling. X-ray diffraction measurements from protein crystals show that proteins fold into very specific conformations. The proper folding is essential for the proteins to perform their biological functions, e.g. for the efficient catalysis of biochemical reactions by specialized proteins—enzymes. Much theoretical effort has been invested in explaining how it is that a protein possesses a single folding state, and how the protein successfully finds it in the sea of all the other possible conformations. Yet, taking into account that the characteristic interaction energies between protein segments are of the order of the characteristic energy of thermal noise, one can suspect that proteins are fluctuating in between different conformations (which are probably all close to some 'perfect' folding state). The biochemical properties of the same protein in different conformations must be different. This leads to the distribution of properties, which is hard to assess by ensemble methods, averaging out individual characteristics. Here the single-molecule methods come to the rescue.

Lu *et al* (1998) measured the chemical kinetics of single cholesterol oxidase (COx) enzymatic activity. The enzymes were trapped in a gel to prevent diffusion and allow long-term monitoring. COx undergoes transitions between a naturally fluorescent state, where COx's active site is oxidized, and a dark state, where the active site is reduced. The turnovers are relatively slow with typical dwell times of $\sim$100 ms for each state. Hence one can reliably distinguish the fluorescent state (on state) from the dark state (off state) in each cycle by measuring the rate of photon emission. After accumulating the time traces of photon counts from individual COx molecules, Lu *et al* (1998) analysed the statistics of on and off times for each of the enzyme molecules. As the turnover process is stochastic, for each molecule there is a distribution of on and off times. The exponential fit to each of the distributions gives the characteristic chemical rate for each molecule. Are these rates identical for all of the molecules? The experimental results by Lu *et al* (1998) showed that different molecules are characterized by different rates of on $\rightarrow$ off transition, and the distribution of the rates is rather broad (static disorder). Notice that all of the molecules are identical in their amino acid sequence. Therefore the difference in the properties arises either from the difference in the conformations of enzyme molecules or from the changes introduced into them after their synthesis (posttranslational modification).

Further, Lu *et al* (1998) addressed the following question: given that there are fluctuations in the chemical rates over ensemble (static disorder), are there fluctuations in the chemical rates over time for the same molecule (dynamic disorder)? The dynamic disorder implies not only that there are different possible conformations in both on and off state, but also that the folding state of a molecule can be different in the different turnovers. However, if the molecules had picked their folding states in the consecutive turnovers completely at random, the enzymatic process would have been characterized by a single averaged chemical rate. So for the dynamic (as well as for the static) disorder the molecules should keep some memory

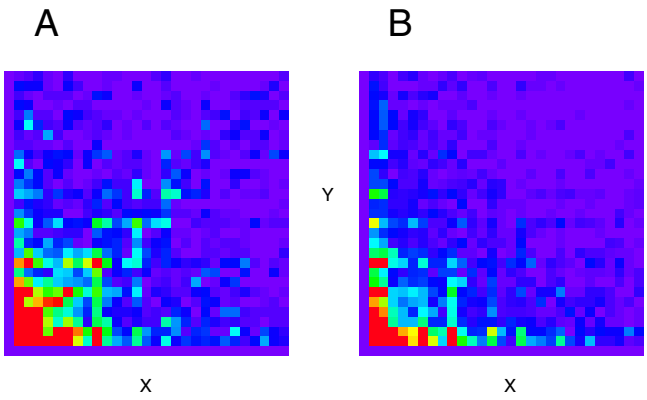

Figure 11. The grey-level coded 2D conditional probability distribution for a pair of on times (x and y) separated by a certain number of turnovers (reprinted with permission from Lu *et al* (1998). Copyright 1998 American Association for the Advancement of Science.) The scale of the x and y axes are from 0 to 1 s. (*A*) The 2D conditional histogram for on times of two adjacent turnovers, which is derived from the trajectories of 33 COx molecules. A subtle diagonal feature is present. (*B*) Same for two on times separated by 10 turnovers. The diagonal feature vanishes because the two on times become independent of each other at the 10-turnover separation. The colour code in (*A*) and (*B*) represents the occurrence (z axis) from 350 (red) to 0 (purple).

(This figure is in colour only in the electronic version)

of their conformations in the preceding turnovers. As Lu *et al* (1998) pointed out, this kind of dynamics is beyond the scope of conventional chemical kinetics, which assumes Markovian processes. The dynamic disorder is impossible to assess with ensemble averaging methods as these measurements cannot distinguish it from the static disorder. Thus the single-molecule approach is warranted in this case.

In principle, the existence of the dynamic disorder can be demonstrated by FCS with the autocorrelation function of fluorescence emission from a single molecule: if the transitions of an enzyme molecule are characterized by single forward and backward rates, the autocorrelation function decays as a single exponential. However, if chemical rates fluctuate the autocorrelation function should decay as a multi-exponential. The latter was the case for the emission of COx. However, Lu *et al* (1998) do not find an FCS analysis convincing enough, as there are other types of fluctuations yielding a multi-exponential autocorrelation function. Thus they suggested another, more definite data processing, showing the existence of dynamic disorder through the statistical analysis of the distribution of lifetimes of the on state. As mentioned above, each of the molecules is characterized by an approximately Poissonian distribution $p(\tau_{on})$ of on times τ_{on}. The transition process is stochastic and the dwell time in the on state as well as in the off state in each turnover is random. The question is if τ_{on} in the consecutive turnovers are correlated. If they are, this would constitute proof of the memory effect. Lu *et al* (1998) assess this through the conditional probability $p(x, y)$ of measuring pairs of on times $\tau_{on} = x$ and y separated by a certain number of turnovers. No correlation between the on times would mean that $p(x, y) = p(x)\, p(y)$. Since $p(\tau_{on})$ is a monotonously decaying function, in the case of no correlation $p(x, y)$ should be a monotonously decaying function of both its parameters. This appears to be the case when measuring on times separated by 10 turnovers (figure 11(b)). However, $p(x, y)$ for adjacent turnovers (figure 11(a)) has a diagonal feature which points to the fact that an enzyme molecule is likely to have similar on times in the consecutive turnovers.

The results can be explained by assuming that the enzyme has at least two conformations E and E', so that there are two possible oxydo-reduction transitions: (1) between the E on state and off state, and (2) between the E' on state and off state. These transitions are characterized by different kinetic rates, which leads to the observed static disorder: different molecules in the ensemble will have different, either E or E', conformations and thus different kinetic rates. The dynamic disorder arises as a result of conformational fluctuations between E and E' for each enzyme molecule. If $E \leftrightarrow E'$ transitions are slower than the oxydo-reduction turnovers, the interchanges between E and E' will result in the observed memory effect with fluctuations of the kinetic rates for a given molecule. The memory effect can be important for the biochemical processes within a cell, as it may lead to non-trivial cooperative effects in the reaction kinetics.

Thus the statistical analysis of fluorescence emission from single molecules allows one to reveal subtle features of chemical kinetics (Lu *et al* 1998), which would have been less accurately analysed by FCS. Similar statistical methods have been applied to other enzymatic systems as well (Edman *et al* 1999, Edman and Rigler 2000).

5.2.2. Diffusion of single molecules. A common misperception in light microscopy is that the precision of an optical measurement cannot go beyond the limits imposed by diffraction (the so-called Abbe limit). However, even though diffraction limits the ability to optically resolve two close objects, it does not preclude the precise measurement of the position of a single object, as demonstrated in single-molecule imaging.

Single-molecule imaging (SMI) is possible with very low concentrations of fluorescent molecules, such that there is less than one molecule per diffraction-limited spot, i.e molecules are separated by more than $\sim$200 nm. In the image plane each molecule is then represented by a spot of light, whose shape is characteristic of the response of the optical system to the point source (this response is named point-spread function, or PSF). This spot can be fitted with PSF to determine the position of the molecule with great precision, which is itself limited only by the number of photons collected per fluorescent molecule and the background noise. Schmidt *et al* (1996) developed this single-molecule imaging scheme to track the diffusion of individual dye-labelled lipid molecules within a lipid bilayer. A highly efficient optical scheme is used to reduce the background scattered light and to collect a maximum of the fluorescence signal with a very sensitive CCD camera. When the concentration of the labelled molecules is low enough, single molecules appear on a CCD array as peaks in the two-dimensional distribution of intensities. Fitting these peaks with Gaussian PSF profiles, Schmidt *et al* (1996) are able to determine the positions of the molecules with a precision of $\sim$30 nm. Furthermore, following the molecule positions over time, the trajectories of individual molecules are visualized. Through the illumination of only a small portion of the CCD and the use of the rest of the CCD chip as a storage device, a time resolution of a few milliseconds is achieved. Then the trajectories are analysed to obtain the kinetics of diffusion of individual molecules.

For a simple lipid bilayer, a diffusion kinetics characteristic of normal diffusion is obtained (Schmidt *et al* 1996). However, for the diffusion within a membrane (Schütz *et al* 2000) of a muscle cell the anomalous diffusion kinetics is observed (figure 12). This kinetics points to the existence of domains within the membrane which restrict the diffusion of the probe. As discussed already in section 4.3, the presence of domains in the cell membrane has major implications for cell functioning.

Thus FCS and SMI techniques give complementary temporal and spatial information. SMI has a spatial resolution of $\sim$30 nm but its resolution in time is limited to a few milliseconds. On the other hand, FCS has a superior temporal resolution (from the nanosecond time scale) but gives only limited spatial information. We expect that FCS and SMI will be implemented

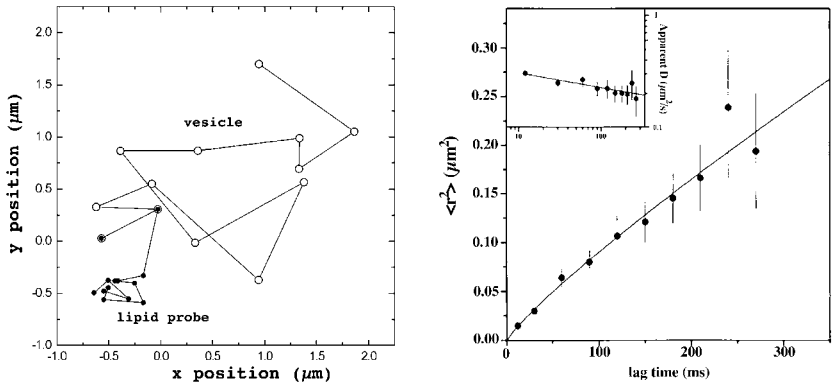

Figure 12. (*A*) Trajectories of the two-dimensional diffusion for a lipid probe embedded within an artificial lipid vesicle (open circles) or within a cell plasma membrane (full circles). (*B*) Mean square displacement of the lipid molecules in the muscle cell membrane shows saturation at long time lags. This behaviour can be explained with the model of restricted diffusion (full curve) (from Schütz *et al* (2000), copyright 2000 European Molecular Biology Organization).

in the same experimental setup in the future, as they conveniently share a number of common features: epi-fluorescence laser illumination, optical filters and sensitive photodetection.

We presented two techniques of single-molecule spectroscopy (section 5.2), as well as the fluorescence intensity distribution analysis (section 5.1), to show how different data processing can complement the autocorrelation analysis of the FCS technique. In fact, the development of the confocal FCS can be considered as a benchmark for later technical developments, refining the statistical analysis of fluorescence emission from a single molecule.

6. Conclusion

In this paper we have reviewed the general theoretical analysis of an FCS measurement, as well as its experimental implementation and successful application during the past decade. FCS is essentially a spectroscopic tool, whose versatility and ease of implementation has opened up new possibilities in experimental statistical physics, biophysics and analytical chemistry.

Even though the analytical formalism developed by Magde *et al* (1972, 1974) requires very little update, the technical improvements associated with the introduction of the confocal geometry, and the improvements of photon detection opened up new applications for FCS. Since its rebirth, FCS has been used to measure translational and rotational mobilities of biomolecules *in vitro* and *in vivo*, to measure the absolute concentrations of fluorescent molecules in living cells, to characterize the photodynamics of fluorescent molecules, as well as to monitor conformational fluctuations of GFP and nucleic acids.

The revival in FCS coincides with the introduction of new paradigms in the biological sciences. The relevance of thermal fluctuations in protein dynamics, as well as the importance of stochastic variation in biological systems, has long been disregarded. However, new experiments, specifically in the protein folding and enzymology fields, are starting to tease out the function of rare fluctuations as a determinant of the viability of a biological system.

For example, studying the kinetics of polymerization of the RecA protein on stretched DNA, Leger *et al* (1998) arrived at the conclusion that RecA monomers bind to the locally extended conformations of DNA arising from spontaneous fluctuations. In the same paradigm, Volkman *et al* (2001) have shown that thermally excited allosteric changes account for

the phosphorylation-driven activation of a signalling protein NtrC. Further examples of the interplay between biomolecular fluctuation and function have been reviewed by Frauenfelder and McMahon (1998) and Kumar *et al* (2000).

As reviewed here, FCS can be successfully implemented to study such biomolecular interactions driven by thermally activated conformational fluctuations. We would like to emphasize that the statistical analysis of the fluctuations, through the auto/cross-correlation function of an associated fluorescence fluctuation, is a non-invasive measurement with rich prospects in biological physics. In the complementary techniques of FCS (FIDA and SMI), an alternative statistical analysis of fluorescence emission provides further insights into the dynamics of biological systems. Future developments of fluorescence statistical analysis will permit physicists to revisit thermal noise as both an obstacle and a driving force in biomolecular complex systems.

Acknowledgments

We wish to thank A Libchaber for support during our introduction to the Fluorescence Correlation Spectroscopy technique. We also wish to thank K Gall, J D Politz, R Rigler, G Schütz, W W Webb and S Xie for allowing the reproduction of their data.

References

Aragón S R and Pecora R 1975 *Biopolymers* **14** 119–38
Auer M, Moore K J, Meyer-Almes F J, Guenther R, Pope A J and Stoeckli K A 1998 *Drug Discovery Today* **3** 457–65
Berland K M 1997 *Biophys. J.* **72** 1487–8
Berland K M, So P T C, Chen Y, Mantulin W W and Gratton E 1996 *Biophys. J.* **71** 410–20
Berland K M, So P T C and Gratton E 1995 *Biophys. J.* **68** 694–701
Berne B J and Peccora R 1976 *Dynamic Light Scattering* (New York: Wiley)
Björling S, Kinjo M, Földes-Papp Z, Hagman E, Thyberg P and Rigler R 1998 *Biochemistry* **37** 12971–8
Bonnet G, Krichevsky O and Libchaber A 1998 *Proc. Natl Acad. Sci. USA* **95** 8602–6
Börsch M, Turina P, Eggeling C, Fries J R, Seidel C A M, Labahn A and Gräber P 1998 *FEBS Lett.* **437** 251–4
Brock R 1998 *Cell Mol. Biol.* **44** 847–56
Brock R, Hink M A and Jovin T M 1998 *Biophys. J.* **75** 2547–57
Cantor C R and Schimmel P R 1980 *Biophysical Chemistry: The Behavior of Biological Macromolecules* (San Francisco: Freeman)
Cantor C R and Smith C L 1999 *Genomics: The Science and Technology Behind the Human Genome Project* (New York: Wiley)
Chen Y, Müller J D, So P T C and Gratton E 1999 *Biophys. J.* **77** 553–67
Clausen-Schaumann H, Seitz M, Krautbauer R and Gaub H E 2000 *Curr. Opin. Chem. Biol.* **4** 524–30
Cluzel P, Surette M and Leibler S 2000 *Science* **287** 1652–5
Craenenbroeck E V and Engelborghs Y 1999 *Biochemistry* **38** 5082–8
Daune M 1999 *Molecular Biophysics: Structures in Motion* (Oxford: Oxford University Press)
Denk W, Stickler J H and Webb W W 1990 *Science* **248** 73–6
Dickson R M, Cubitt A B, Tsien R Y and Moerner W E 1997 *Nature* **388** 355–8
Dorn I T, Neumaier K R and Tampé R 1998 *J. Am. Chem. Soc.* **120** 2753–63
Edman L, Földes-Papp Z, Wennmalm S and Rigler R 1999 *Chem. Phys.* **247** 11–21
Edman L, Mets Ü and Rigler R 1996 *Proc. Natl Acad. Sci. USA* **93** 6710–15
Edman L and Rigler R 2000 *Proc. Natl Acad. Sci. USA* **97** 8266–71
Eggeling C, Widengren J, Rigler R and Seidel C A M 1998 *Anal. Chem.* **70** 2651–9
Ehrenberg M and Rigler R 1974 *Chem. Phys.* **4** 390–401
Eigen M and Rigler R 1994 *Proc. Natl Acad. Sci. USA* **91** 5740–7
Einstein A 1905 *Ann. Phys., Lpz.* **17** 549
Elson E L and Magde D 1974 *Biopolymers* **13** 1–27
Fahey P F, Koppel D E, Barak L S, Wolf D E, Elson E L and Webb W W 1975 *Science* **195** 305–6
Fahey P F and Webb W W 1978 *Biochemistry* **17** 3046–53

Frauenfelder H and McMahon B 1998 *Proc. Natl Acad. Sci. USA* **95** 4795–7
Gennerich A and Schild D 2000 *Biophys. J.* **79** 3294–306
Goddard N, Bonnet G, Krichevsky O and Libchaber A 2000 *Phys. Rev. Lett.* **85** 2400
Häsler K, Pänke O and Junge W 1999 *Biochemistry* **38** 13 759–65
Haupts U, Maiti S, Schwille P and Webb W W 1998 *Proc. Natl Acad. Sci. USA* **95** 13 573–8
Heikal A A, Hess S T, Baird G S, Tsien R Y and Webb W W 2000 *Proc. Natl Acad. Sci. USA* **97** 11 996–2001
Heinze K G, Koltermann A and Schwille P 2000 *Proc. Natl Acad. Sci. USA* **97** 10 377–82
Hermansson G T 1996 *Bioconjugate Techniques* (San Diego, CA: Academic)
Hillisch A, Lorenz M and Diekmann S 2001 *Curr. Opin. Struct. Biol.* **11** 201–7
Huang Z and Thompson N L 1996 *Biophys. J.* **70** 2001–7
Kask P, Günther R and Axhausen P 1997 *Eur. Biophys. J.* **25** 163–9
Kask P, Palo K, Fay N, Brand L, Mets Ü, Ullmann D, Jungmann J, Pschorr J and Gall K 2000 *Biophys. J.* **78** 1703–13
Kask P, Palo K, Ullmann D and Gall K 1999 *Proc. Natl Acad. Sci. USA* **96** 13 756–61
Kinjo M and Rigler R 1995 *Nucleic Acids Res.* **23** 1795–9
Kneen M, Farinas J, Li Y and Verkman A S 1998 *Biophys. J.* **74** 1591–9
Koppel D E 1974 *Phys. Rev.* A **10** 1938–45
Korlach J, Schwille P, Webb W W and Feigenson G W 1999 *Proc. Natl Acad. Sci. USA* **96** 8461–6
Kumar S, Ma B, Tsai C J, Sinha N and Nussinov R 2000 *Protein Sci.* **9** 10–19
Lamb D C, Schenk A, Röcker C, Scalfi-Happ C and Nienhaus G U 2000 *Biophys. J.* **79** 1129–38
Leger J F, Robert J, Bourdieu L, Chatenay D and Marko J F 1998 *Proc. Natl Acad. Sci. USA* **95** 12 295–9
Llopis J, McCaffery J M, Miyawaki A, Farquhar M G and Tsien R Y 1998 *Proc. Natl Acad. Sci. USA* **95** 6803–8
Lu H P, Xun L and Xie X S 1998 *Science* **282** 1877–82
Magde D, Elson E and Webb W W 1972 *Phys. Rev. Lett.* **29** 705–8
Magde D, Elson E L and Webb W W 1974 *Biopolymers* **13**
Maiti S, Haupts U and Webb W W 1997 *Proc. Natl Acad. Sci. USA* **94** 11 753–7
Mehta A D, Rief M, Spudich J A, Smith D A and Simmons R M 1999 *Science* **283** 1689–95
Meseth U, Wohland T, Rigler R and Vogel H 1999 *Biophys. J.* **76** 1619–31
Mets Ü, Widengren J and Rigler R 1997 *Chem. Phys.* **218** 191–8
Meyer-Almes F-J, Wyzgol K and Powell M J 1998 *Biophys. Chem.* **75** 151–60
Miesenbock G, De Angelis D A and Rothman J E 1998 *Nature* **394** 192–5
Müller J D, Chen Y and Gratton E 2000 *Biophys. J.* **78** 474–86
Pack C-G, Nishimura G, Tamura M, Aoki K, Taguchi H, Yoshida M and Kinjo M 1999 *Cytometry* **36** 247–53
Palo K, Mets Ü, Jäger S, Kask P and Gall K 2000 *Biophys. J.* **79** 2858–66
Perrin J 1914 *The Atoms* (Leipzig: Lottermoser)
Petersen N O 1986 *Biophys. J.* **49**
Petersen N O, Hoddelius P L, Wiseman P W, Seger O and Magnusson K E 1993 *Biophys. J.* **49** 1135–46
Petersen N O, Johnson D C and Schlesinger M J 1986 *Biophys. J.* **49** 809–15
Politz J C, Browne E S, Wolf D E and Pederson T 1998 *Proc. Natl Acad. Sci. USA* **95** 6043–8
Pramanik A, Thyberg P and Rigler R 2000 *Chem. Phys. Lipids* **104** 35–47
Qian H 1990 *Biophys. Chem.* **38** 49–57
Qian H and Elson E L 1990a *Proc. Natl Acad. Sci. USA* **87** 5479–83
Qian H and Elson E L 1990b *Biophys. J.* **57** 375–80
Rigler R and Elson E S 2001 *Fluorescence Correlation Spectroscopy (Springer Series in Chemical Physics)*, vol 65 (New York: Springer)
Rigler R, Mets Ü, Widengren J and Kask P 1993 *Eur. J. Biophys.* **22** 169–75
Rigler R, Widengren W and Mets Ü 1992 *Fluorescence Spectroscopy. New Methods and Applications* ed O Wolfbeis (Berlin: Springer) pp 13–24
Schlessinger J, Axelrod D, Koppel D E, Webb W W and Elson E L 1975 *Science* **195** 307–9
Schmidt T, Hinterdorfer P and Schindler H 1999 *Microsc. Res. Tech.* **44** 339–46
Schmidt T, Schülz G J, Baumgartner W, Gruber H J and Schindler H 1996 *Proc. Natl Acad. Sci. USA* **93** 2926–9
Schrof W, Klingler J F, Rozouvan S and Horn D 1998 *Phys. Rev.* E **57** R2523–6
Schüler J, Frank J, Trier U, Schäfer-Korting M and Saenger W 1999 *Biochemistry* **38** 8402–8
Schürer H, Buchynskyy A, Korn K, Famulok M, Welzel P and Hahn U 2001 *Biol. Chem.* **382** 479–81
Schütz G J, Kada G, Pastushenko V P and Schindler H 2000 *EMBO J.* **19** 892–901
Schwille P, Haupts U, Maiti S and Webb W W 1999a *Biophys. J.* **77** 2251–65
Schwille P, Korlach J and Webb W W 1999b *Cytometry* **36** 176–82
Schwille P, Kummer S, Heikal A A, Moerner W E and Webb W W 2000 *Proc. Natl Acad. Sci. USA* **97** 151–6
Schwille P, Meyer-Almes F-J and Rigler R 1997 *Biophys. J.* **72** 1878–86

Schwille P, Oehlenschläger F and Walter N G 1996 *Biochemistry* **35** 10 182–93
Srivastava M and Petersen N O 1998 *Biophys. Chem.* **75** 201–11
Strick T, Allemand J-F, Bensimon D and Croquette V 2000 *Ann. Rev. Biophys. Biomol. Struct.* **29** 523–43
Takakuwa Y, Pack C-G, An X-L, Manno S, Ito E and Kinjo M 1999 *Biophys. Chem.* **82** 149–55
Thompson N L 1991 *Topics in Fluorescence Spectroscopy Techniques* vol 1, ed J R Lakowicz (New York: Plenum) pp 337–78
Thompson N L and Axelrod D 1983 *Biophys. J.* **43** 103–14
Thompson N L, Burghardt T P and Axelrod D 1981 *Biophys. J.* **33** 435–54
Tsien R Y 1998 *Ann. Rev. Biochem.* **67** 509–44
Tyagi S and Kramer F R 1996 *Nature Biotech.* **14** 303–8
Volkman B F, Lipson D, Wemmer D E and Kern D 2001 *Science* **291** 2429–33
Wachsmuth M, Waldeck W and Langowski J 2000 *J. Mol. Biol.* **298** 677–89
Wang J, Sood A K, Satyam P V, Feng Y, Wu X-Z, Cai Z, Yun W and Sinha S K 1998 *Phys. Rev. Lett.* **80** 1110–13
Weiss S 1999 *Science* **283** 1676–83
Weiss S 2000 *Nat. Struct. Biol.* **7** 724–9
Wennmalm S, Edman L and Rigler R 1997 *Proc. Natl Acad. Sci. USA* **94** 10 641–6
Widengren J, Dapprich J and Rigler R 1997 *Chem. Phys.* **6** 417–26
Widengren J, Mets Ü and Rigler R 1995 *J. Phys. Chem.* **99** 13 368–79
Widengren J, Mets Ü and Rigler R 1999a *Chem. Phys.* **250** 171–86
Widengren J, Terry B and Rigler R 1999b *Chem. Phys.* **249** 259–71
Winkler T, Kettling U, Koltermann A and Eigen M 1999 *Proc. Natl Acad. Sci. USA* **96** 1375–8
Wiseman P W and Petersen N O 1999 *Biophys. J.* **76** 963–77
Wohland T, Friedrich K, Hovius R and Vogel* H 1999 *Biochemistry* **38** 8671–81
Xie X S and Lu H P 1999 *J. Biol. Chem.* **274** 15 967–70
Xie X S and Trautman J K 1998 *Ann. Rev. Phys. Chem.* **49** 441–80
Yanagida T, Kitamura K, Tanaka H, Iwane A H and Esaki S 2000 *Curr. Opin. Cell Biol.* **12** 20–5